Enhanced Aerosol Mass in the Tropical Tropopause Layer Linked to Ozone Abundance

Shang Liu[1], Troy Dean Thornberry[2], Pengfei Yu[3], Sarah Woods[4], Karen H. Rosenlof[5], and Ru-Shan Gao[6]

[1]Northeastern University
[2]NOAA ESRL
[3]Institute for Environmental and Climate Research, Jinan University
[4]National Center for Atmospheric Research
[5]NOAA ESRL CSL
[6]NOAA Chemical Sciences Laboratory

December 3, 2023

Abstract

Aerosol particles play a critical role in the tropical tropopause layer (TTL) through cloud formation and heterogeneous chemistry, influencing the radiative and chemical balance of the stratosphere. However, aerosol measurements in the TTL are sparse, resulting in poor knowledge of aerosol abundance and distribution in this important region. Here, we present in situ aircraft measurements over the western tropical Pacific, revealing a persistent and altitude-dependent enhancement of aerosol mass in the TTL compared to the convectively influenced troposphere below. Notably, our data demonstrate a striking positive correlation between aerosol mass and ozone. Model simulations suggest that organic materials constitute a substantial fraction of the total aerosol mass within the TTL. We further derived an empirical parameterization of TTL aerosol mass as a function of ozone. Given the relative ease of ozone measurements and modeling, the parameterization provides a promising framework for estimating TTL aerosol abundance and its effects on climate.

Enhanced Aerosol Mass in the Tropical Tropopause Layer Linked to Ozone Abundance

Shang Liu[1,*], Troy D. Thornberry[2], Pengfei Yu[3], Sarah Woods[4], Karen H. Rosenlof[2], and Ru-Shan Gao[2,*]

[1]Department of Civil and Environmental Engineering, Northeastern University, Boston, MA 02115, USA
[2]NOAA Chemical Sciences Laboratory, Boulder, CO, USA
[3]Institute for Environmental and Climate Research, Jinan University, Guangzhou, China
[4]Earth Observing Laboratory, National Center for Atmospheric Research (NCAR), Boulder, CO

*Correspondence author: shang.liu@northeastern.edu, rushan.gao@noaa.gov

Key Points:

- Aircraft measurements reveal persistent enhancement of aerosol mass in the TTL.
- The TTL aerosol enhancement tightly correlates with ozone. An empirical parameterization of TTL aerosol as a function of ozone is derived.
- Modeling suggests that TTL aerosol particles are mainly composed of organics and sulfate.

Abstract

Aerosol particles play a critical role in the tropical tropopause layer (TTL) through cloud formation and heterogeneous chemistry, influencing the radiative and chemical balance of the stratosphere. However, aerosol measurements in the TTL are sparse, resulting in poor knowledge of aerosol abundance and distribution in this important region. Here, we present in situ aircraft measurements over the western tropical Pacific, revealing a persistent and altitude-dependent enhancement of aerosol mass in the TTL compared to the convectively influenced troposphere below. Notably, our data demonstrate a striking positive correlation between aerosol mass and ozone. Model simulations suggest that organic materials constitute a substantial fraction of the total aerosol mass within the TTL. We further derived an empirical parameterization of TTL aerosol mass as a function of ozone. Given the relative ease of ozone measurements and modeling, the parameterization provides a promising framework for estimating TTL aerosol abundance and its effects on climate.

Plain Language Summary

We investigated tiny particles called aerosols in a specific atmospheric layer called the tropical tropopause layer (TTL). These particles are crucial because they affect cloud formation and chemical processes in the atmosphere, influencing how energy is distributed. Unfortunately, there hasn't been much research on aerosols in the TTL, leading to gaps in our understanding of their abundance and distribution in this important region. To fill this knowledge gap, we conducted measurements using aircraft over the western tropical Pacific. Our findings revealed that aerosol

mass in the TTL is consistently higher compared to the lower troposphere, which is influenced by upward air movement. What's interesting is that we observed a clear connection between the amount of aerosol and ozone. Our model simulations indicated that a significant portion of the aerosol mass in the TTL is made up of organic materials. To make it easier to estimate aerosol levels and their impact on climate, we developed a way to predict TTL aerosol mass based on ozone measurements. Since ozone is relatively straightforward to measure and model, our method could provide a useful framework for understanding aerosol abundance in the TTL and its effects on the climate.

1 Introduction

As the main pathway for the transport of tropospheric air into the stratosphere, the TTL largely determines the entry values for the materials entering the stratosphere (Fueglistaler et al., 2009). The properties of the TTL air and the processes occurring in the TTL thus affect the global stratosphere and climate (Randel and Jensen, 2013; SPARC 2006).

Aerosol particles in the TTL affect the stratospheric water vapor budget through TTL dehydration processes by serving as nuclei for the formation of cirrus clouds (Penner et al., 2009). TTL circus clouds have substantial impacts on the earth's radiative balance (Hong et al., 2016). By providing condensed surface areas, TTL aerosol can also facilitate condensation of low vapor pressure gases such as sulfuric acid (Brock et al., 1995) and promote heterogeneous chemistry that depletes ozone once they are transported to the stratosphere (Tolbert et al., 1988). Despite the importance, the abundance and properties of the TTL aerosol remain poorly characterized. Field observations have suggested that new particle formation events frequently occur in the TTL, in particular the lower TTL just below the tropopause (Brock et al., 1995; Weigel et al., 2011, 2021). The composition of the TTL aerosol is influenced by tropical dynamics (e.g., transport) and regional continental air sources (Froyd et al., 2009). Recent advancements in SO_2 measurement in the TTL suggests little contribution of SO_2 to stratospheric aerosols, revealing a significant gap in the stratospheric aerosol budget (Rollins et al., 2017). The complex dynamic and chemical processes in the TTL make it difficult to elucidate the formation mechanisms of the TTL aerosol. In-situ measurements of TTL aerosol are limited, hindering our understanding on the climate impacts of the TTL and stratospheric aerosols.

For this study, we carried out aircraft measurements of aerosols over the western Pacific warm pool during the Pacific Oxidants, Sulfur, Ice, Dehydration, and cONvection (POSIDON) campaign in October 2016. The western Pacific warm pool plays a leading role for transport of air into the TTL (Fueglistaler et al., 2005). Our measurements were carried out during nine flights aboard a NASA WB-57F high-altitude aircraft stationed in Guam. Throughout these flights, we extensively characterized TTL aerosols and trace gases (flight tracks are shown in Fig. 1). To complement the measurements, we employed modeling techniques to obtain insights into the chemical composition of the aerosols. The combined approach of aerosol measurements, tracer analysis, and modeling offers insight into aerosol abundance and formation mechanisms within the TTL.

2 Methods

2.1 Measurements

The POSIDON campaign, took place during October 2016, aimed at improving our understanding of the physical and chemical processes occurring in the TTL. A total of nine flights were carried out on board the NASA WB-57 high altitude aircraft from Guam (13.5° N, 144.8° E). These flights covered the region from 0 to 15°N and from 130 to 160° E (Fig. 1a), with vertical coverage spanning 0 to19 km (Fig. 1b). Each flight path consisted of several upward and downward segments between 14 and 18 kilometers in altitude, providing extensive sampling of the TTL. The measurement region lies over the tropical warm pool, where high sea surface temperatures lead to widespread deep atmospheric convection (Yan et al., 1992).

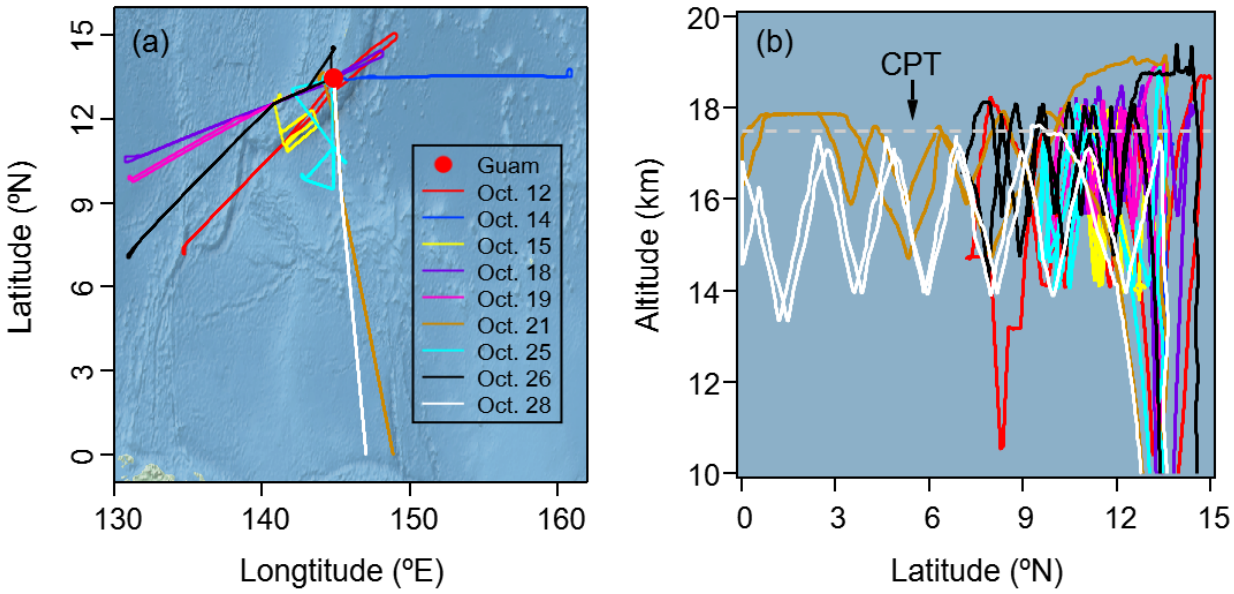

Figure 1. Flight tracks during the POSIDON campaign.

The aerosol particles were sampled through a near-isokinetic inlet that reduces the ambient sample speed from the aircraft speed of ~90–200 m s^{-1} to ~3 m s^{-1} while maintaining ambient aerosol mixing ratios (Jonsson et al., 1995). This inlet has been employed in various aircraft campaigns for aerosol sampling (e.g. Schwarz et al., 2006). Aerosol number size distribution was measured in situ by a custom-built optical particle counter, the portable optical particle spectrometer (POPS), which was mounted in the fuselage bay of the aircraft. The POPS uses a 405 nm laser to count and size individual aerosol particles with diameters from 140 to 3000 nm (Gao et al., 2016). The scientific application of the POPS has been demonstrated by recent field campaigns (Cui et al., 2018; Liu et al., 2021; Yu et al., 2017). In the POPS instrument, each particle passing across the laser beam produces a pulse by scattering the laser light. The particle number is determined by the number of the pulses. The particle size is calculated from the intensity of the pulse, which was calibrated using a series of differential mobility analyzer (DMA) size-selected dioctyl sebacate (DOS) particles prior to the campaign. The aerosol mass was calculated from the aerosol number and size assuming that the particles are spherical and have a constant density of 1.6 g cm^{-3}. The

mass mixing ratio (MMR) of aerosols was determined as the ratio of aerosol mass to the density of ambient air, which was calculated from the measured air pressure and temperature. A lognormal fit to the measured mass size distribution derived from the POPS measurements in the TTL (Fig. S1) suggests that the POPS measurements captured approximately 50% of the total aerosol mass. Laboratory tests suggest that the POPS instrument used during POSIDON can provide reliable measurements under pressures as low as 70 hPa, which corresponds to an altitude of 18.9 km in this study. Therefore the POPS data acquired above 18.9 km are not used in the analysis.

The size distribution of particles with diameter larger than 3 μm was measured with a fast cloud droplet probe (FCDP). The FCDP detects particle forward scattering to determine the number and size of particles (Lance et al., 2010; McFarquhar et al., 2007). We assume that all particles greater than 3 μm are ice crystals as the number of large aerosol particles in the upper troposphere is negligible (Jensen et al., 2013). We found that ice crystals could likely abrade the inlet materials, resulting in artifacts in POPS-measured aerosol size distribution. Such interference has been observed in previous aircraft measurements (Murphy et al., 2004). For this reason, we excluded the POPS data when ice crystals were present from the analysis.

Additional real-time measurements included: (i) ozone mixing ratio obtained using a custom UV spectrophotometer designed for high altitude airborne deployment with high accuracy and precision (Gao et al., 2012), (ii) water vapor mixing ratio measured by a two-channel tunable diode laser-based hygrometer, which is capable of accurately measuring low-concentration (below 1 ppm) water vapor in the upper troposphere and lower stratosphere (Thornberry et al., 2015), and (iii) ambient air pressure and temperature measured by the Meteorological Measurement System (MMS; Chan et al., 1989; Scott et al., 1990), which also records aircraft position with 1-second time resolution.

2.2 Modeling

We employed the Community Aerosol and Radiation Model for Atmospheres (CARMA), an advanced sectional aerosol model (Toon et al., 1988; Yu et al., 2015). CARMA is coupled with the Community Earth System Model (CESM), allowing for comprehensive analysis of aerosols. The model operates at a spatial resolution of 1.9° × 2.5° and employs a time step of 30 minutes. The model incorporates 35 vertical pressure levels, spanning from the Earth's surface up to 200 hPa, and an additional 21 vertical pressure levels from 200 hPa to 2 hPa. Simulations are nudged to meteorology from Modern-Era Retrospective analysis for Research and Applications, Version 2 (MERRA-2; Gelaro et al., 2017).

CARMA tracks two groups of aerosols, with each group containing 20 size bins. The first group consists of pure sulfate particles with aerosol diameter ranging from 0.4 nm to 2.6 μm. These particles form through nucleation and condensation of water and sulfuric acid vapor (Zhao and Turco, 1995). The second group comprises internally mixed aerosols with the diameters varying from 100 nm to 17 μm. These mixed aerosols consist of particles that contain organic compounds, black carbon (BC), sea salt, dust, and condensed sulfate.

In addition, we employed a straightforward, observationally constrained chemical model to characterize the vertical distribution of O_3 within the TTL. This model is a one-dimensional column model that allows updrafts and vertical mixing but assumes no horizontal mixing. The O_3 formation process is represented using the Chapman mechanism, and O_3 profiles were calculated for the altitude range of 14.5–18.9 km. A detailed description of the model is provided in the Supporting Information.

3 Results and discussion

3.1 Determination of TTL

We adopt the upper boundary of the TTL to be at 19 km, following SPARC (2006). This altitude is 2.5 km higher than the cold point tropopause (CPT) as shown in Fig. S2. The CPT corresponds to an altitude of 17.5 km and air temperature of approximately 190 K. These values are in line with previous measurements of TTL (Fueglistaler et al., 2009; Gettelman et al., 2004).

The lower boundary of the TTL is determined by examining the vertical profile of potential temperature (θ; Fig. S3). The curvature of the altitude-θ profile changes at 14.5 km, which is mathematically characterized as the lapse rate minimum (LRM) of θ. This change reflects the transition of stability regimes, i.e., deep convection dominates air stability below the LRM and radiation starts to influence air temperature above the LRM. Accordingly, we identify the LRM level at 14.5 km (355 K, 140 hPa) as the base of the TTL (Gettelman and Forster, 2002), which is consistent with previous studies (Fueglistaler et al., 2009; Sunilkumar et al., 2017). As a result, the TTL spans from 14.5 km to 20 km, and the majority of our measurements were conducted within the TTL (Fig. 1).

3.2 Vertical profile of aerosols and ozone

The vertical profile of aerosol mass from the surface to the top of the TTL can be segmented in three layers with distinct characteristics (Fig. 2a). Layer I spans from the surface to 5 km altitude and represents the lower troposphere, in which the MMR of aerosols decreased logarithmically with altitude from 2 μg kg^{-1} to 0.08 μg kg^{-1} likely because of the influence of surface emissions from Guam. Layer II ranges from 5 km to 14.5 km altitude. In this layer, the aerosol MMR remained at approximately 0.08 μg kg^{-1} with small variability. Such low-concentration aerosol layers immediately below the convection outflow have been observed previously over the Northern Indian Ocean (de Reus et al., 2001) and the rain forests in South America (Andreae et al., 2018; Krejci et al., 2003). The observation indicates that deep convection serves as an effective sink for aerosol particles (Yu et al., 2019). Layer III lies in the TTL, extending from 14.5 km to 18.9 km, with the upper boundary 1.4 km higher than the CPT. In this layer the aerosol MMR increased rapidly from 0.08 μg kg^{-1} at 14.5 km to 1.5 μg kg^{-1} at 18.9 km. Our observations show a sustained increase of aerosol MMR from the upper troposphere to lower stratosphere across the tropopause, rather than abrupt transitions. This suggests that the CPT has no unique role for the transport of aerosols. Accounting for the mass of <140 nm particles that were not measured by the POPS instrument, the aerosol MMR at 18.9 km would be approximately 3 μg kg^{-1}. This concentration is close to the measurement during the POLARIS mission in 1997 (Mclinden et al.,

1999), in which an aerosol MMR of approximately 3.5 μg kg^{-1} was observed for aerosols with size range of 0.07–1 μm at 18.9 km in eastern Pacific (17.5° N, 159.3° W).

The ozone concentration remained below 35 ppb in layers I and II and began to increase at 14.5 km (Fig. 2b). This observation is consistent with previous ozonesonde measurements in the tropical Pacific (Folkins et al., 1999; Folkins and Martin, 2005). The concurrence of ozone minimum and LRM is in line with the analysis by Gettelman and Forster (2002) and Folkins et al. (2002).

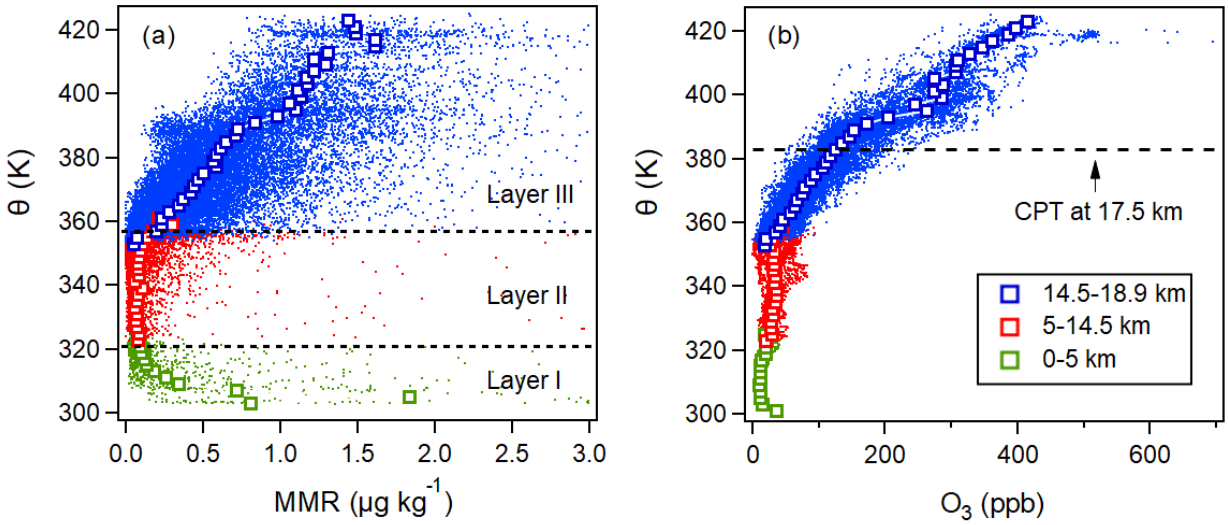

Figure 2. Potential temperature (θ) versus **(a)** O_3 and **(b)** MMR for data acquired from 0–5 km, 5–14.5 km, and 14.5–18.9 km measurements for all flights. Individual data points (5-s averages) are shown by the dots and the averages (by θ of 2K) are shown by the solid squares.

3.3 Mechanisms for aerosol enhancement in the TTL

We find that the aerosol MMR was tightly correlated with O_3 in the TTL during all flights with small variation between flights. This can be clearly seen in the example time series of O3 and aerosol MMR for the flight on October 18 shown in Fig. 3a. The Pearson's correlation coefficient (r) for the campaign-average O_3 and aerosol MMR (averaged into 2-K θ intervals) was 0.98 in layer III. In contrast, the aerosol MMR and O_3 were anticorrelated with an r value of -0.35 in layer I (Fig. 3b), and no correlation was observed between aerosol MMR and O_3 in layer II.

The main processes contributing to the increase in TTL O_3 from the bottom to the top of the TTL include chemical production via photolytic dissociation of molecular oxygen (O_2) (Prather 2009; Crutzen et al., 1999) and isentropic in-mixing of stratospheric air from the extratropical lower stratosphere (Konopka et al., 2010; Ploeger et al., 2012). The relative contribution of these processes to O_3 remains unclear. While some studies argue that in situ chemical production dominates (Avallone and Prather 1996), others suggest that isentropic stratospheric in-mixing can contribute to O_3 by as much as 40-60% (Abalos et al., 2013a, 2013b; Konopka et al., 2009, 2010; Ploeger et al., 2011, 2012; Sargent et al., 2014). This contribution is most significant during the boreal summer months (June–August), primarily driven by the Asian summer monsoon, and

gradually decreases during transition into the fall and winter months. In particular, these studies suggest that the contribution from in-mixing falls within the range of 0-20% in October, averaged over a ±10°N latitude range, with the contribution increasing with altitude.

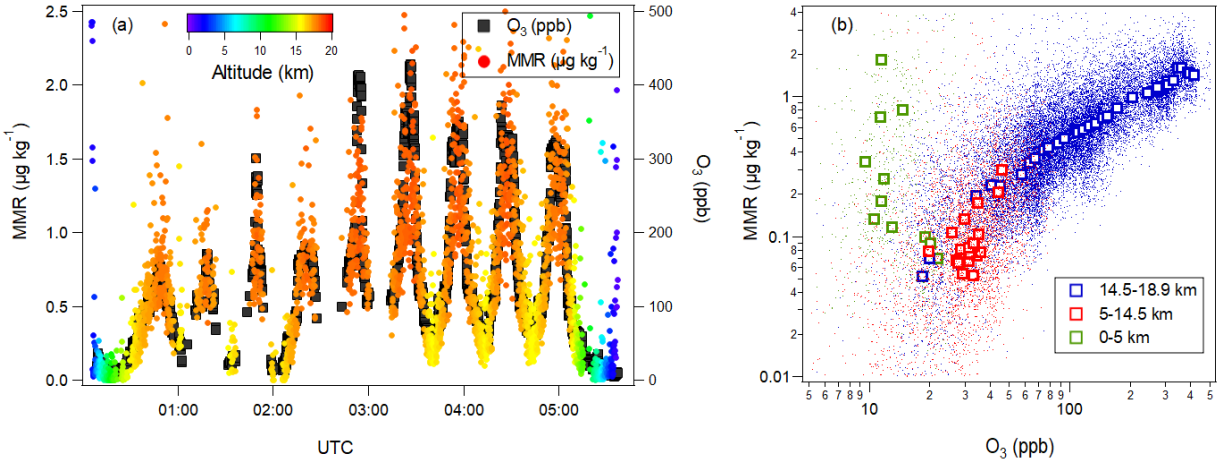

Figure 3. **(a)** Example time series of aerosol MMR and O_3 for the October 18 measurements. The gaps indicate ice-influenced data that were excluded from the analysis. **(b)** Scatter plot of MMR vs O_3 for the 0–5 km (layer I), 5–14.5 km (layer II), and 14.5–18.9 km (layer III) measurements. Individual data points are shown by the dots and the averages are shown by the solid squares Logarithmic scales are used to make the small values visible.

We used a one-dimensional column model (over the flight region) and tracer analysis to examine these processes. The model calculates the vertical distribution of O_3 within the TTL, considering a constant slow vertical ascent rate of 0.25 mm s^{-1} (Park et al., 2010; Avallone and Prather 1996) of air in the TTL and assuming it evolves in isolation (Supporting Information). Remarkably, the calculated vertical profile of O_3 closely aligns with the observed O_3 profile (Fig. 4a). This result is in line with earlier investigations that yielded similar results using a column model (Avallone and Prather 1996) and with research that assumed the tropics are isolated from extra-tropics when explaining the annual cycles of ozone above the tropical tropopause (Randel et al., 2007; Schoeberl et al., 2008). However, we acknowledge the simplicity of the model. For example, the model does not consider the chemistry of nitrogen oxides (NO and NO_2; not measured during POSIDON) and O_3, which could be important in the TTL O_3 abundance (Nussbaumer et al., 2023), and uncertainties exist in the assumed ascent rate. On the other hand, the tracer analysis shows evidence of stratospheric in-mixing. Fig. S4 shows that N_2O was anticorrelated with O_3 in the TTL during POSIDON. The observed negative correlation indicates that the sampled TTL air included a contribution from mixing of stratospheric origin (Folkins et al., 1999). This is because the strong UV radiation at higher altitudes in the stratosphere photolyzes N_2O while leading to O_3 production, resulting in an anticorrelation of N_2O and O_3 (Assonov et al., 2013). In contrast, N_2O in the troposphere is inert and uniformly distributed, thus correlation of N_2O with O_3 is not expected and not observed below the TTL during our measurements. The synthesis of modeling and tracer analysis indicates contributions from both chemical production and stratospheric in-mixing to TTL

O_3. Given the strong correlation between O_3 and aerosols in the TTL, these results suggest that TTL aerosols may also come from a combination of these chemical and physical processes.

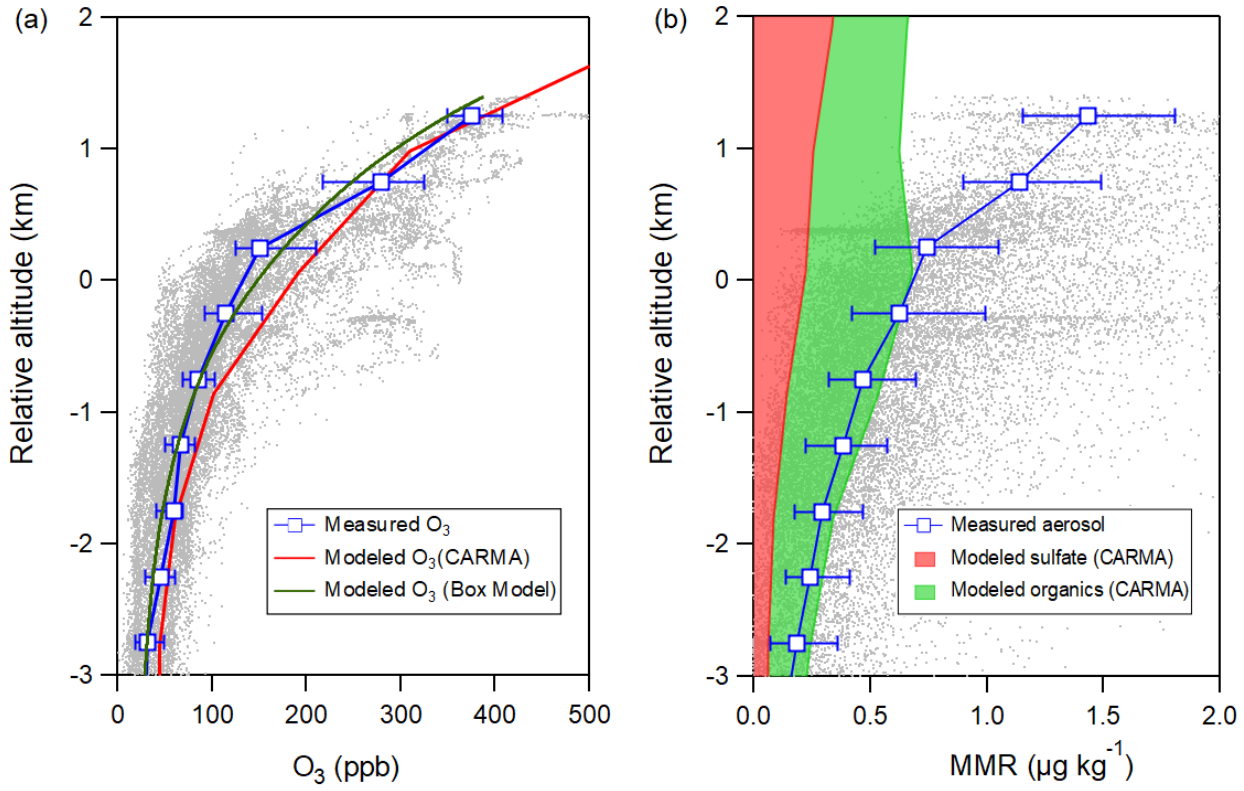

Figure 4. Comparison of modeling results to measurements for **(a)** O_3 and **(b)** aerosol MMR. Individual measurement points are shown by the grey dots. The median values and the 25th and 75th percentiles are shown by the blue line-square symbols and the error bars. The y-axis represents altitude relative to the tropopause.

To investigate the chemical composition of TTL aerosol, we employed the CARMA model embedded in CESM to simulate the aerosol formation and growth processes. The model reproduced the O_3 profile reasonably well (Fig. 4a). Our model results suggest that sulfate aerosol exhibits a consistent increase with altitude, whereas organic aerosol displays an ascending trend below the tropopause but declines above it. Moreover, our modeled vertical profile of the total aerosol MMR demonstrates good agreement with the in situ measurements (Fig. 4b) below the tropopause, with organic aerosol constituting the significant fraction of the aerosol mass. These modeling results imply that sulfur alone is insufficient to explain the observed aerosol mass, and organic precursors may play a pivotal role in the formation and/or growth of TTL aerosols under low-temperature conditions. This finding aligns with previous findings from TTL measurements during the Pre-AVE and CR-AVE campaigns over Southwest Central America in boreal winter (Froyd et al., 2009), which highlighted the prevalence of organic-sulfate particles as the most abundant particle type in the TTL and lower stratosphere. We note that the model underestimates the aerosol mass above the tropopause, with the difference increasing with altitude within the TTL,

reaching 60% at an altitude of 1 km above the CPT. Additional research is needed to understand this discrepancy.

We postulate that TTL aerosols are likely generated through the processes of new particle formation and subsequent growth following convective outflow in the upper troposphere (Williamson et al., 2019). The observed aerosol number size distribution in the TTL suggests particle growth with increasing altitude (Fig. S5), although obtaining measurements of smaller particles would enhance our understanding. During convective transport, soluble species are effectively removed, whereas the insoluble and weakly soluble species can endure washout and gradually ascend upward, with minimal loss, to reach the stratosphere (Bechara et al., 2010). The TTL, characterized by low temperature, low particle surface area density, and high relative humidity, provides ideal conditions for new particle formation and growth. Multiple studies have proposed the upper troposphere as the primary nucleation region (Brock et al., 1995; Weigel et al., 2011), and investigations have revealed the involvement of organics in new particle formation and initial growth in the remote tropical upper troposphere (Kupc et al., 2020). Future measurements analyzing the composition of oxidized organic species will enhance our understanding of particle formation and growth pathways. Exceptional overshooting that crosses the tropical tropopause could also affect the aerosol abundance in the TTL (Vernier et al., 2011). This possibility is examined using H_2O as a tracer. The θ-H_2O profile displayed no spikes above the tropopause (Fig. S6), suggesting the absence of overshooting during the measurements.

The prevalence of secondary aerosol formation as the primary factor influencing TTL aerosol abundance is in line with the strong correlation between TTL aerosol mass and O_3 in our measurements. Building upon this observation and the underlying mechanisms, we further derived an empirical parameterization of aerosol MMR as a function of O_3 in the TTL using linear regression. The derived relationship is expressed as MMR ($\mu g\ kg^{-1}$) = $0.0074(\pm 2.2 \times 10^{-4}) \times O_3$ (ppb) + 0.23 ($\pm$0.049), accounting for the 50% mass that was not measured by the POPS instrument. This parameterization could be used to estimate TTL aerosol abundance and for validation of modeled results.

4 Conclusions

Our aircraft measurements conducted over the western Pacific revealed a vertically stratified aerosol distribution comprised of three distinct layers. The lower-troposphere layer, ranging from 0 to 5 km in altitude, exhibited a decrease in aerosol mass with height, primarily influenced by surface-level emissions. The layer between 5 and 14.5 km displayed consistently low aerosol concentrations with minimal variability, indicating effective aerosol removal through deep convection processes. In the TTL, we observed an enhanced aerosol mass that exhibited a strong correlation with O_3. The modeling and tracer analysis suggest that TTL O_3 and aerosols likely originate from a combination of chemical production and stratospheric in-mixing processes. Furthermore, based on the linear relationship observed between aerosol MMR and O_3 in the TTL, we derived an empirical parameterization that allows for the estimation of aerosol MMR as a

function of O_3. This parameterization holds potential for validating the simulated TTL aerosol abundance in global models, enabling the simulation of the climate impacts of TTL aerosols.

Our study also highlights the challenge of accurately predicting aerosol mass, particularly above the tropopause, even for the most advanced models. This underscores the existence of significant gaps in our understanding of the origin and formation mechanisms of aerosols in the TTL. To achieve a more comprehensive understanding of TTL aerosol, it is crucial to conduct future measurements that encompass detailed aerosol chemical composition and gas-phase precursors across different locations and seasons. These endeavors will help diagnose potential deficiencies in the models and validate the modeling results. Consequently, they will lead to an improved comprehension of TTL aerosols and facilitate a predictive understanding of their effects on stratospheric chemistry, clouds, and climate.

Acknowledgement

We appreciate the funding support from ERB. We would like to thank Paul Lawson from APEC Incorporated for the help with collecting the FCDP data. We are also thankful to Paul Bui for providing the MMS data.

Data Availability Statement

The aircraft measurements during the POSIDON field campaign are available through the NASA ESPO Data Archive: https://espoarchive.nasa.gov/archive/browse/posidon/WB57

References

Abalos, M., Randel, W.J., Kinnison, D.E., & Serrano, E. (2013). Quantifying tracer transport in the tropical lower stratosphere using WACCM. *Atmos. Chem. Phys*., 13, 10591–10607.

Abalos et al., Ploeger, F., Konopka, P., Randel, W. J., & Serrano, E. (2013). Ozone seasonality above the tropical tropopause: reconciling the Eulerian and Lagrangian perspectives of transport processes, *Atmos. Chem. Phys.*, 13, 10787–10794.

Andreae, M. O., Afchine, A., Albrecht, R., Holanda, B. A., Artaxo, P., Barbosa, H. M. J., et al. (2018). Aerosol characteristics and particle production in the upper troposphere over the Amazon Basin. *Atmo. Meas. Tech.*, 18, 921–961.

Assonov, S. S., Brenninkmeijer, C. A. M., Schuck, T. & Umezawa, T. (2013). N_2O as a tracer of mixing stratospheric and tropospheric air based on CARIBIC data with applications for CO_2. *Atmos. Environ.*, 79, 769–779.

Avallone, L. M., & Prather, M., J. (1996). Photochemical evolution of ozone in the lower tropical stratosphere. *J. Geophys. Res.*, 101. https://doi.org/10.1029/95JD03010.

Bechara, J., Borbon, A., Jambert, C., Colomb, A., & Perros, P. E. (2010). Evidence of the impact of deep convection on reactive volatile organic compounds in the upper tropical troposphere during the AMMA experiment in West Africa. *Atmos. Chem. Phys.*, 10, 10321–10334.

Brock, C. A., Hamill, P., Wilson, J. C., Jonsson, H. H., & Chan, K. R. (1995). Particle formation in the upper tropical troposphere : A Source of Nuclei for the Stratospheric Aerosol. *Science*, 270, 1650–1653.

Chan, K. R., Scott, S. G., & Bui, T. P. (1989). Temperature and horizontal wind measurements on the ER-2 aircraft during the 1987 airborne Antarctic ozone experiment. *J. Geophys. Res.*, 94, 11573–11587. https://doi.org/10.1029/JD094iD09p11573.

Cui, Y. Y., Liu, S., Bai, Z., Bian, J., Li, D., Fan, K. et al. (2018). Religious burning as a potential major source of atmospheric fine aerosols in summertime Lhasa on the Tibetan Plateau. *Atmos. Environ.*, 181, 186–191.

Crutzen, P. J., Lawrence, M. G., & Poschl, U. (1999). On the background photochemistry of tropospheric ozone. *Tellus*, 51A-B, 123–146.

Folkins, I. & Martin, R. V. (2005). The vertical structure of tropical convection and its impact on the budgets of water vapor and ozone. *J. Atmos. Sci.*, 62(5), 1560–1573.

Folkins, I., Loewenstein, M., Podolske, J., & Oltmans, J. (1999). A barrier to vertical mixing at 14 km in the tropics: Evidence from ozonesondes and aircraft measurements. *J. Geophys. Res.*, 104, 22095–22102. https://doi.org/10.1029/1999JD900404.

Folkins, I., Braun, C., Thompson, A. M., & Witte, J. (2002). Tropical ozone as an indicator of deep convection. *J. Geophys. Res. Atmos.*, 107(13), 1–10. https://doi.org/10.1029/2001JD001178.

Froyd, K. D., Murphy, D. M., Sanford, T. J., Thomson, D. S., Wilson, J. C., Pfister, L., & Lait, L. (2009). Aerosol composition of the tropical upper troposphere. *Atmos. Chem. Phys.*, 9, 4363–4385.

Fueglistaler, S., M. Bonazzola, P. H. Haynes, & Peter T. (2005). Stratospheric water vapor predicted from the Lagrangian temperature history of air entering the stratosphere in the tropics. *J. Geophys. Res.*, 110, D08107, doi:10.1029/2004JD005516.

Fueglistaler, S., Dessler, A. E., Dunkerton, T. J., Folkins, I., Fu, Q., & Mote, P. W. (2009). Tropical tropopause layer. *Rev. Geophys.*, 47, https://doi.org/10.1029/2008RG000267.

Gao, R. S., Ballard, J., Watts, L. A., Thornberry, T. D., Ciciora, S. J., McLaughlin, R. J., & Fahey, D. W. (2012). A compact, fast UV photometer for measurement of ozone from research aircraft, *Atmos. Meas. Tech.*, 5(9), 2201–2210. https://doi.org/10.5194/amt-5-2201-2012.

Gao, R. S., Telg, H., McLaughlin, R. J., Ciciora, S. J., Watts, L. A., Richardson, M. S. et al. (2016). A light-weight, high-sensitivity particle spectrometer for $PM_{2.5}$ aerosol measurements. *Aerosol Sci. Technol.*, 50, 88–99..

Gettelman, A. & Forster, P. M. d. F. (2002). A climatology of the tropical tropopause layer. *J. Meteorol. Soc. Japan*, 80(4B), 911–924. https://doi.org/10.2151/jmsj.80.911.

Hong, Y., Liu, G., & Li, J.-L. F. (2016). Assessing the radiative effects of global ice clouds based on CloudSat and CALIPSO measurements. *J. Climate*, 7651–7674, https://doi.org/10.1175/JCLI-D-15-0799.1.

Jensen, E. J., Diskin, G., Lawson, R. P., Lance, S., Bui, T. P., Hlavka, D. et al. (2013). Ice nucleation and dehydration in the tropical tropopause layer. *Proc. Natl. Acad. Sci.*, 110(6). https://doi/org/10.1073/pnas.1217104110.

Jonsson, H. H., Wilson, J. C., Brock, C. A., Knollenberg, R. G., Newton, R., Dye, J. E. et al. (1995). Performance of a focused cavity aerosol spectrometer for measurements in the stratosphere of particle size in the 0.06-2.0-µm-dimaeter range. *J. Atmos. Ocean. Technol.*, 12, 115–129.

Konopka, P., Grooß, J.-U., Ploeger, F., & Müller, R. (2009). Annual cycleof horizontal in-mixing into the lower tropical stratosphere. *J. Geophys. Res.*, 114, D19111. https://doi.org/10.1029/2009JD011955.

Konopka, P., Grooß, J.-U., Günther, G., Ploeger, F., Pommrich, R., Müller, R., & Livesey, N. (2010). Annual cycle of ozone at and above thetropical tropopause: Observations versus simulations with the ChemicalLagrangian Model of the Stratosphere (CLaMS). *Atmos. Chem. Phys.*,10, 121–132.

Krejci, R., Stro, J., Reus, M. De, Hoor, P., Williams, J. & Fischer, H. (2003). Evolution of aerosol properties over the rain forest in Surinam , South America , observed from aircraft during the LBA-CLAIRE 98 experiment. *J. Geophys. Res.-Atmos*, 108, 1–17. doi:10.1029/2001JD001375.

Kupc, A., Williamson, C. J., Hodshire, A. L., Kazil, J., Ray, E., Bui, T. P. et al. (2020). The potential role of organics in new particle formation and initial growth in the remote tropical upper troposphere. *Atmos. Chem. Phys.*, 20, 15037–15060.

Lance, S., Brock, C. A., Rogers, D., Gordon, J. A., & Oceanic, N. (2010). Water droplet calibration of the Cloud Droplet Probe (CDP) and in-flight performance in liquid , ice and mixed-phase clouds during ARCPAC. *Atmo. Meas. Tech.*, 3, 1683–1706. https://doi:10.5194/amt-3-1683-2010.

Mcfarquhar, G. M., Um, J., Freer, M., Baumgardner, D., Kok, G. L., & Mace, G. (2007). Importance of small ice crystals to cirrus properties: Observations from the Tropical Warm Pool International Cloud Experiment. *Geophys. Res. Lett.*, 34, 1–6. https://doi.org/10.1029/2007GL029865.

Liu, S., Liu, C. C., Froyd K. D., Schill, G. P., Murphy, D. M., Bui, T. P. et al. (2021). Sea spray aerosol concentration modulated by sea surface temperature. *Proc. Natl. Acad. Sci.*, 118(9), https://doi.org/10.1073/pnas. 2020583118.

Mclinden, C. A., McConnell, J. C., McElroy, C. T., & Griffioen, E. (1999). Observations of stratospheric aerosol using CPFM polarized limb radiances. *J. Atmos. Sci.*, 56, 233–240.

Murphy, D. M., Cziczo, D. J., Hudson, P. K., Thomson, D. S., Wilson, J. C., Buseck, P. R. et al. (2004). Particle generation and resuspension in aircraft inlets when flying in clouds particle

generation and resuspension in aircraft inlets when flying in clouds. *Aerosol Sci. Technol.*, 38, 401–409. https://doi.org/10.1080/02786820490443094.

Nussbaumer, C. M., Fischer, H., Lelieveld, J., & Pozzer, A. (2003). What controls ozone sensitivity in the upper tropical troposphere? *Atmos. Chem. Phys*., 23, 12651–12669.

Penner, J. E., Chen, Y., Wang, M., & Liu, X. (2009). Possible influence of anthropogenic aerosols on cirrus clouds and anthropogenic forcing. *Atmos. Chem. Phys*., 9(3), 879–896. https://doi.org/10.5194/acp-9-879-2009.

Ploeger, F., fueglistaler, S., Grooß, J.-U., Günther, G., Konopka, P., Liu, Y. S., et al. (2011). Insight from ozone and water vapour on transportin the tropical tropopause layer (TTL). *Atmos. Chem. Phys*, 11, 407–419.

Ploeger, F., Konopka, P., Müller, R., Fueglistaler, S., Schmidt, T., Manners, J. C. et al. (2012). Horizontal transport affecting trace gas seasonality in the Tropical Tropopause Layer (TTL). *J. Geophys. Res.*, 117, D09303. https://doi.org/10.1029/2011JD017267.

Prather, M. J. (2009). Tropospheric O_3 from photolysis of O_2. *Geophys. Res. Lett.*, 36. https://doi:10.1029/2008GL036851.

Randel, W. J. & Jensen, E. J. (2013). Physical processes in the tropical tropopause layer and their roles in a changing climate. *Nat. Geosci.*, 6, 169–176. https://doi/org10.1038/ngeo1733.

Randel, W. J., Park, M., & Wu, F. (2007). A large annual cycle in ozone above the tropical tropopause linked to the Brewer-Dobson circulation. *J. Atmos. Sci.*, 4479–4488.

de Reus, M., Krejci, R., Williams, J., Fischer, H., Scheele, R. & Strom, J. (2001). Vertical and horizontal distributions of the aerosol number concentration and size distribution over the northern Indian Ocean. *J. Geophys. Res.-Atmos*, 106, 629–641. https://doi.org/10.1029/2001JD900017.

Gelaro, R., McCarty, W., Suarez, M. J., Todling, R., Molod, A., Takacs, L. et al. (2017). The Modern-Era Retrospective Analysis for Research and Applications, Version 2 (MERRA-2). *J. Climate*, 5419–5454.

Rollins, A. W., Thornberry, T. D., Watts, L. A., Yu, P., Rosenlof, K. H., Mills, M. et al. (2017). The role of sulfur dioxide in stratospheric aerosol formation evaluated by using in situ measurements in the tropical lower stratosphere. *Geophys. Res. Lett*., 4280–4286. https:// doi.org/10.1002/2017GL072754.

Sargent, M. R., Smith, J. B., Sayres, D. S., & Anderson, J. G. (2014). The roles of deep convection and extratropical mixing in the tropical tropopause layer: An in situ measurement perspective. *J. Geophys. Res.-Atmos*, 12355–12371. https://doi.org/10.1002/2014JD022157.

Schoeberl, M. R., Douglass, A. R., Newman, P. A., Lait, L. R., Lary, D., Waters, J. (2008). QBO and annual cycle variations in tropical lower stratosphere trace gases from HALOE and Aura MLS observations. *J. Geophys. Res.*, 113, D05301. https://doi.org/10.1029/2007JD008678.

Schwarz, J. P., Gao, R. S., Fahey, D. W., Thomson, D. S., Watts, L. A., Wilson, J. C. (2006). Single-particle measurements of midlatitude black carbon and light-scattering aerosols from the boundary layer to the lower stratosphere. *J. Geophys. Res*., 111. https://doi.org/10.1029/2006JD007076, doi:10.1029/2006JD007076.

Scott, S. G., Bui, P. T. & Chan, R. K. (1990). The meteorological measurement system on the NASA ER-2 aircraft. *J. Atmos. Ocean. Technol.*, 7, 525–540.

Stratosphere-troposphere Processes and their Role in Climate (SPARC), Assessment of Stratospheric Aerosol Properties (ASAP), WCRP-124, WMO/TD No. 1295, SPARC Rep. 4, 2006.

Sunilkumar, S. V., Muhsin, M., Venkat Ratnam, M., Parameswaran, K., Krishna Murthy, B. V., & Emmanuel, M. (2017). Boundaries of tropical tropopause layer (TTL): A new perspective based on thermal and stability profiles. *J. Geophys. Res*., 741–754, 2017. https://doi.org/10.1002/2016JD025217.

Thornberry, T. D., Rollins, A. W., Gao, R. S., Watts, L. A., Ciciora, S. J., McLaughlin, & Fahey, D. W. (2015). A two-channel, tunable diode laser-based hygrometer for measurement of water vapor and cirrus cloud ice water content in the upper troposphere and lower stratosphere. *Atmos. Meas. Tech.*, 8, 211-224. https://doi.org/10.5194/amt-8-211-2015.

Tolbert, A., Rossi, J. M. & Golden, D. M. (1988). Heterogeneous interactions of chlorine nitrate, hydrogen chloride, and nitric acid with sulfuric acid surfaces at stratospheric temperatures. *Geophys. Res. Lett.*, 15, 847–850. https://doi.org/10.1029/GL015i008p00847.

Toon, O. B., Turco, R. P., Westphal, D., Malone, R., & Liu, M. (1988). A multidimensional model for aerosols—Description of computational analogs. *Journal of the Atmospheric Sciences*, 45(15), 2123–2144.

Vernier, J., Pommereau, J., Thomason, L. W., Pelon, J., Garnier, A., Deshler, T. et al. (2011). Overshooting of clean tropospheric air in the tropical lower stratosphere as seen by the CALIPSO lidar. *Atmos. Chem. Phys.*, 9683–9696. https://doi.org/10.5194/acp-11-9683-2011.

Weigel, R., Borrmann, S., Kazil, J., Minikin, A., Stohl, A., Wilson, J. C. et al. (2011). In situ observations of new particle formation in the tropical upper troposphere: The role of clouds and the nucleation mechanism. *Atmos. Chem. Phys.*, 11, 9983–10010. https://doi.org/10.5194/acp-11-9983-2011.

Weigel, R., Mahnke, C., Baumgartner, M., Dragoneas, A., Vogel, B., Ploeger, F. et al. (2021). In situ observation of new particle formation (NPF) in the tropical tropopause layer of the 2017 Asian monsoon anticyclone – Part 1:Summary of StratoClim results. *Atmos. Chem. Phys*., 21, 11689–11722.

Williamson, C. J., Kupc, A., Axisa, D., Bilsback, K. R., Bui, T., Campuzano-jost, P. (2019). A large source of cloud condensation nuclei from new particle formation in the tropics. *Nature*, 574,

399–403. https://doi.org/10.1038/s41586-019-1638-9.

Yan, X., Ho, C., Zheng, Q., & Klemas, V. (1992). Temperature and size variabilities of the western pacific warm pool. *Science,* 258, 1643–1645.

Yu, P., Toon, O. B., Bardeen, C. G., Mills, M. J., Fan, T., English, J. M., & Neely, R. R. (2015). Evaluations of tropospheric aerosol properties simulated by the community Earth system model with a sectional aerosol microphysics scheme. *Journal of Advances in Modeling Earth Systems, 7*(2), 865–914.

Yu, P., Rosenlof, K. H., Liu, S., Telg, H., Thornberry, T. D., Rollins, A. W. et al. (2017). Efficient transport of tropospheric aerosol into the stratosphere via the Asian summer monsoon anticyclone. *Proc. Natl. Acad. Sci.*, 114(27), 6972–6977. https://doi.org/10.1073/pnas.1701170114.

Yu, P., Froyd, K. D., Portmann, R. W., Toon, O. B., Freitas, S. R., Bardeen, C. G. et al. (2019). Efficient in-cloud removal of aerosols by deep convection. Geophysical Research Letters, 46. https://doi.org/10.1029/2018GL080544.

Zhao, J., & Turco, R. P. (1995). Nucleation simulations in the wake of a jet aircraft in stratospheric flight. *J. Aerosol Sci.*, 26, 779–795.

Enhanced Aerosol Mass in the Tropical Tropopause Layer Linked to Ozone Abundance

Shang Liu[1,*], Troy D. Thornberry[2], Pengfei Yu[3], Sarah Woods[4], Karen H. Rosenlof[2], and Ru-Shan Gao[2,*]

[1]Department of Civil and Environmental Engineering, Northeastern University, Boston, MA 02115, USA
[2]NOAA Chemical Sciences Laboratory, Boulder, CO, USA
[3]Institute for Environmental and Climate Research, Jinan University, Guangzhou, China
[4]Earth Observing Laboratory, National Center for Atmospheric Research (NCAR), Boulder, CO

*Correspondence author: shang.liu@northeastern.edu, rushan.gao@noaa.gov

Key Points:

- Aircraft measurements reveal persistent enhancement of aerosol mass in the TTL.
- The TTL aerosol enhancement tightly correlates with ozone. An empirical parameterization of TTL aerosol as a function of ozone is derived.
- Modeling suggests that TTL aerosol particles are mainly composed of organics and sulfate.

Abstract

Aerosol particles play a critical role in the tropical tropopause layer (TTL) through cloud formation and heterogeneous chemistry, influencing the radiative and chemical balance of the stratosphere. However, aerosol measurements in the TTL are sparse, resulting in poor knowledge of aerosol abundance and distribution in this important region. Here, we present in situ aircraft measurements over the western tropical Pacific, revealing a persistent and altitude-dependent enhancement of aerosol mass in the TTL compared to the convectively influenced troposphere below. Notably, our data demonstrate a striking positive correlation between aerosol mass and ozone. Model simulations suggest that organic materials constitute a substantial fraction of the total aerosol mass within the TTL. We further derived an empirical parameterization of TTL aerosol mass as a function of ozone. Given the relative ease of ozone measurements and modeling, the parameterization provides a promising framework for estimating TTL aerosol abundance and its effects on climate.

Plain Language Summary

We investigated tiny particles called aerosols in a specific atmospheric layer called the tropical tropopause layer (TTL). These particles are crucial because they affect cloud formation and chemical processes in the atmosphere, influencing how energy is distributed. Unfortunately, there hasn't been much research on aerosols in the TTL, leading to gaps in our understanding of their abundance and distribution in this important region. To fill this knowledge gap, we conducted measurements using aircraft over the western tropical Pacific. Our findings revealed that aerosol

mass in the TTL is consistently higher compared to the lower troposphere, which is influenced by upward air movement. What's interesting is that we observed a clear connection between the amount of aerosol and ozone. Our model simulations indicated that a significant portion of the aerosol mass in the TTL is made up of organic materials. To make it easier to estimate aerosol levels and their impact on climate, we developed a way to predict TTL aerosol mass based on ozone measurements. Since ozone is relatively straightforward to measure and model, our method could provide a useful framework for understanding aerosol abundance in the TTL and its effects on the climate.

1 Introduction

As the main pathway for the transport of tropospheric air into the stratosphere, the TTL largely determines the entry values for the materials entering the stratosphere (Fueglistaler et al., 2009). The properties of the TTL air and the processes occurring in the TTL thus affect the global stratosphere and climate (Randel and Jensen, 2013; SPARC 2006).

Aerosol particles in the TTL affect the stratospheric water vapor budget through TTL dehydration processes by serving as nuclei for the formation of cirrus clouds (Penner et al., 2009). TTL circus clouds have substantial impacts on the earth's radiative balance (Hong et al., 2016). By providing condensed surface areas, TTL aerosol can also facilitate condensation of low vapor pressure gases such as sulfuric acid (Brock et al., 1995) and promote heterogeneous chemistry that depletes ozone once they are transported to the stratosphere (Tolbert et al., 1988). Despite the importance, the abundance and properties of the TTL aerosol remain poorly characterized. Field observations have suggested that new particle formation events frequently occur in the TTL, in particular the lower TTL just below the tropopause (Brock et al., 1995; Weigel et al., 2011, 2021). The composition of the TTL aerosol is influenced by tropical dynamics (e.g., transport) and regional continental air sources (Froyd et al., 2009). Recent advancements in SO_2 measurement in the TTL suggests little contribution of SO_2 to stratospheric aerosols, revealing a significant gap in the stratospheric aerosol budget (Rollins et al., 2017). The complex dynamic and chemical processes in the TTL make it difficult to elucidate the formation mechanisms of the TTL aerosol. In-situ measurements of TTL aerosol are limited, hindering our understanding on the climate impacts of the TTL and stratospheric aerosols.

For this study, we carried out aircraft measurements of aerosols over the western Pacific warm pool during the Pacific Oxidants, Sulfur, Ice, Dehydration, and cONvection (POSIDON) campaign in October 2016. The western Pacific warm pool plays a leading role for transport of air into the TTL (Fueglistaler et al., 2005). Our measurements were carried out during nine flights aboard a NASA WB-57F high-altitude aircraft stationed in Guam. Throughout these flights, we extensively characterized TTL aerosols and trace gases (flight tracks are shown in Fig. 1). To complement the measurements, we employed modeling techniques to obtain insights into the chemical composition of the aerosols. The combined approach of aerosol measurements, tracer analysis, and modeling offers insight into aerosol abundance and formation mechanisms within the TTL.

2 Methods

2.1 Measurements

The POSIDON campaign, took place during October 2016, aimed at improving our understanding of the physical and chemical processes occurring in the TTL. A total of nine flights were carried out on board the NASA WB-57 high altitude aircraft from Guam (13.5° N, 144.8° E). These flights covered the region from 0 to 15°N and from 130 to 160° E (Fig. 1a), with vertical coverage spanning 0 to19 km (Fig. 1b). Each flight path consisted of several upward and downward segments between 14 and 18 kilometers in altitude, providing extensive sampling of the TTL. The measurement region lies over the tropical warm pool, where high sea surface temperatures lead to widespread deep atmospheric convection (Yan et al., 1992).

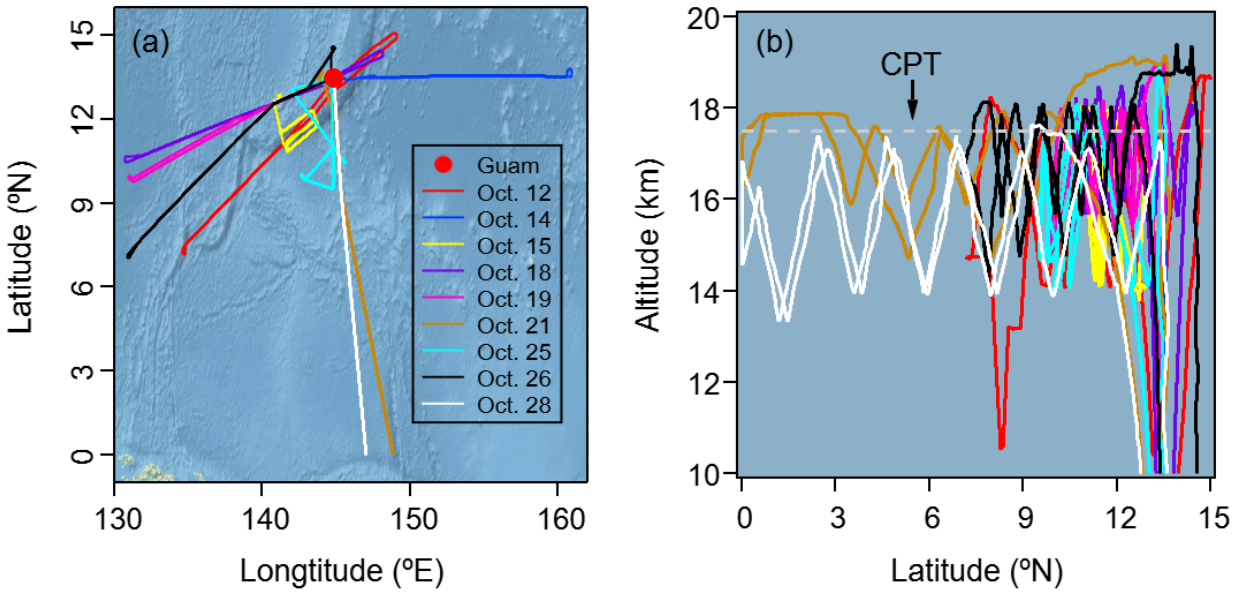

Figure 1. Flight tracks during the POSIDON campaign.

The aerosol particles were sampled through a near-isokinetic inlet that reduces the ambient sample speed from the aircraft speed of ~90–200 m s^{-1} to ~3 m s^{-1} while maintaining ambient aerosol mixing ratios (Jonsson et al., 1995). This inlet has been employed in various aircraft campaigns for aerosol sampling (e.g. Schwarz et al., 2006). Aerosol number size distribution was measured in situ by a custom-built optical particle counter, the portable optical particle spectrometer (POPS), which was mounted in the fuselage bay of the aircraft. The POPS uses a 405 nm laser to count and size individual aerosol particles with diameters from 140 to 3000 nm (Gao et al., 2016). The scientific application of the POPS has been demonstrated by recent field campaigns (Cui et al., 2018; Liu et al., 2021; Yu et al., 2017). In the POPS instrument, each particle passing across the laser beam produces a pulse by scattering the laser light. The particle number is determined by the number of the pulses. The particle size is calculated from the intensity of the pulse, which was calibrated using a series of differential mobility analyzer (DMA) size-selected dioctyl sebacate (DOS) particles prior to the campaign. The aerosol mass was calculated from the aerosol number and size assuming that the particles are spherical and have a constant density of 1.6 g cm^{-3}. The

mass mixing ratio (MMR) of aerosols was determined as the ratio of aerosol mass to the density of ambient air, which was calculated from the measured air pressure and temperature. A lognormal fit to the measured mass size distribution derived from the POPS measurements in the TTL (Fig. S1) suggests that the POPS measurements captured approximately 50% of the total aerosol mass. Laboratory tests suggest that the POPS instrument used during POSIDON can provide reliable measurements under pressures as low as 70 hPa, which corresponds to an altitude of 18.9 km in this study. Therefore the POPS data acquired above 18.9 km are not used in the analysis.

The size distribution of particles with diameter larger than 3 μm was measured with a fast cloud droplet probe (FCDP). The FCDP detects particle forward scattering to determine the number and size of particles (Lance et al., 2010; McFarquhar et al., 2007). We assume that all particles greater than 3 μm are ice crystals as the number of large aerosol particles in the upper troposphere is negligible (Jensen et al., 2013). We found that ice crystals could likely abrade the inlet materials, resulting in artifacts in POPS-measured aerosol size distribution. Such interference has been observed in previous aircraft measurements (Murphy et al., 2004). For this reason, we excluded the POPS data when ice crystals were present from the analysis.

Additional real-time measurements included: (i) ozone mixing ratio obtained using a custom UV spectrophotometer designed for high altitude airborne deployment with high accuracy and precision (Gao et al., 2012), (ii) water vapor mixing ratio measured by a two-channel tunable diode laser-based hygrometer, which is capable of accurately measuring low-concentration (below 1 ppm) water vapor in the upper troposphere and lower stratosphere (Thornberry et al., 2015), and (iii) ambient air pressure and temperature measured by the Meteorological Measurement System (MMS; Chan et al., 1989; Scott et al., 1990), which also records aircraft position with 1-second time resolution.

2.2 Modeling

We employed the Community Aerosol and Radiation Model for Atmospheres (CARMA), an advanced sectional aerosol model (Toon et al., 1988; Yu et al., 2015). CARMA is coupled with the Community Earth System Model (CESM), allowing for comprehensive analysis of aerosols. The model operates at a spatial resolution of 1.9° × 2.5° and employs a time step of 30 minutes. The model incorporates 35 vertical pressure levels, spanning from the Earth's surface up to 200 hPa, and an additional 21 vertical pressure levels from 200 hPa to 2 hPa. Simulations are nudged to meteorology from Modern-Era Retrospective analysis for Research and Applications, Version 2 (MERRA-2; Gelaro et al., 2017).

CARMA tracks two groups of aerosols, with each group containing 20 size bins. The first group consists of pure sulfate particles with aerosol diameter ranging from 0.4 nm to 2.6 μm. These particles form through nucleation and condensation of water and sulfuric acid vapor (Zhao and Turco, 1995). The second group comprises internally mixed aerosols with the diameters varying from 100 nm to 17 μm. These mixed aerosols consist of particles that contain organic compounds, black carbon (BC), sea salt, dust, and condensed sulfate.

In addition, we employed a straightforward, observationally constrained chemical model to characterize the vertical distribution of O_3 within the TTL. This model is a one-dimensional column model that allows updrafts and vertical mixing but assumes no horizontal mixing. The O_3 formation process is represented using the Chapman mechanism, and O_3 profiles were calculated for the altitude range of 14.5–18.9 km. A detailed description of the model is provided in the Supporting Information.

3 Results and discussion

3.1 Determination of TTL

We adopt the upper boundary of the TTL to be at 19 km, following SPARC (2006). This altitude is 2.5 km higher than the cold point tropopause (CPT) as shown in Fig. S2. The CPT corresponds to an altitude of 17.5 km and air temperature of approximately 190 K. These values are in line with previous measurements of TTL (Fueglistaler et al., 2009; Gettelman et al., 2004).

The lower boundary of the TTL is determined by examining the vertical profile of potential temperature (θ; Fig. S3). The curvature of the altitude-θ profile changes at 14.5 km, which is mathematically characterized as the lapse rate minimum (LRM) of θ. This change reflects the transition of stability regimes, i.e., deep convection dominates air stability below the LRM and radiation starts to influence air temperature above the LRM. Accordingly, we identify the LRM level at 14.5 km (355 K, 140 hPa) as the base of the TTL (Gettelman and Forster, 2002), which is consistent with previous studies (Fueglistaler et al., 2009; Sunilkumar et al., 2017). As a result, the TTL spans from 14.5 km to 20 km, and the majority of our measurements were conducted within the TTL (Fig. 1).

3.2 Vertical profile of aerosols and ozone

The vertical profile of aerosol mass from the surface to the top of the TTL can be segmented in three layers with distinct characteristics (Fig. 2a). Layer I spans from the surface to 5 km altitude and represents the lower troposphere, in which the MMR of aerosols decreased logarithmically with altitude from 2 μg kg^{-1} to 0.08 μg kg^{-1} likely because of the influence of surface emissions from Guam. Layer II ranges from 5 km to 14.5 km altitude. In this layer, the aerosol MMR remained at approximately 0.08 μg kg^{-1} with small variability. Such low-concentration aerosol layers immediately below the convection outflow have been observed previously over the Northern Indian Ocean (de Reus et al., 2001) and the rain forests in South America (Andreae et al., 2018; Krejci et al., 2003). The observation indicates that deep convection serves as an effective sink for aerosol particles (Yu et al., 2019). Layer III lies in the TTL, extending from 14.5 km to 18.9 km, with the upper boundary 1.4 km higher than the CPT. In this layer the aerosol MMR increased rapidly from 0.08 μg kg^{-1} at 14.5 km to 1.5 μg kg^{-1} at 18.9 km. Our observations show a sustained increase of aerosol MMR from the upper troposphere to lower stratosphere across the tropopause, rather than abrupt transitions. This suggests that the CPT has no unique role for the transport of aerosols. Accounting for the mass of <140 nm particles that were not measured by the POPS instrument, the aerosol MMR at 18.9 km would be approximately 3 μg kg^{-1}. This concentration is close to the measurement during the POLARIS mission in 1997 (Mclinden et al.,

1999), in which an aerosol MMR of approximately 3.5 μg kg^{-1} was observed for aerosols with size range of 0.07–1 μm at 18.9 km in eastern Pacific (17.5° N, 159.3° W).

The ozone concentration remained below 35 ppb in layers I and II and began to increase at 14.5 km (Fig. 2b). This observation is consistent with previous ozonesonde measurements in the tropical Pacific (Folkins et al., 1999; Folkins and Martin, 2005). The concurrence of ozone minimum and LRM is in line with the analysis by Gettelman and Forster (2002) and Folkins et al. (2002).

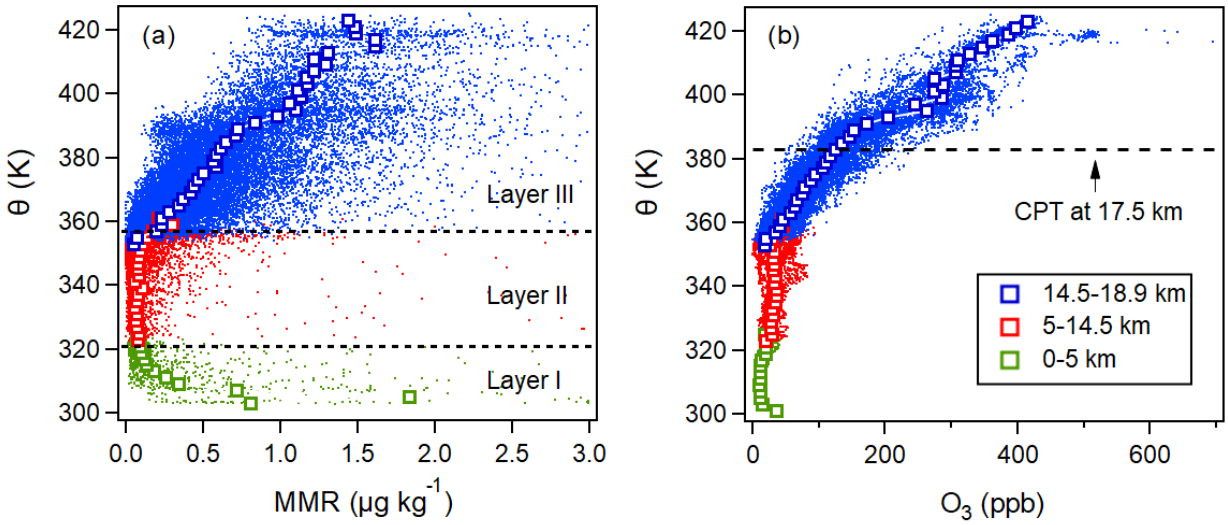

Figure 2. Potential temperature (θ) versus **(a)** O_3 and **(b)** MMR for data acquired from 0–5 km, 5–14.5 km, and 14.5–18.9 km measurements for all flights. Individual data points (5-s averages) are shown by the dots and the averages (by θ of 2K) are shown by the solid squares.

3.3 Mechanisms for aerosol enhancement in the TTL

We find that the aerosol MMR was tightly correlated with O_3 in the TTL during all flights with small variation between flights. This can be clearly seen in the example time series of O3 and aerosol MMR for the flight on October 18 shown in Fig. 3a. The Pearson's correlation coefficient (r) for the campaign-average O_3 and aerosol MMR (averaged into 2-K θ intervals) was 0.98 in layer III. In contrast, the aerosol MMR and O_3 were anticorrelated with an r value of -0.35 in layer I (Fig. 3b), and no correlation was observed between aerosol MMR and O_3 in layer II.

The main processes contributing to the increase in TTL O_3 from the bottom to the top of the TTL include chemical production via photolytic dissociation of molecular oxygen (O_2) (Prather 2009; Crutzen et al., 1999) and isentropic in-mixing of stratospheric air from the extratropical lower stratosphere (Konopka et al., 2010; Ploeger et al., 2012). The relative contribution of these processes to O_3 remains unclear. While some studies argue that in situ chemical production dominates (Avallone and Prather 1996), others suggest that isentropic stratospheric in-mixing can contribute to O_3 by as much as 40-60% (Abalos et al., 2013a, 2013b; Konopka et al., 2009, 2010; Ploeger et al., 2011, 2012; Sargent et al., 2014). This contribution is most significant during the boreal summer months (June–August), primarily driven by the Asian summer monsoon, and

gradually decreases during transition into the fall and winter months. In particular, these studies suggest that the contribution from in-mixing falls within the range of 0-20% in October, averaged over a ±10°N latitude range, with the contribution increasing with altitude.

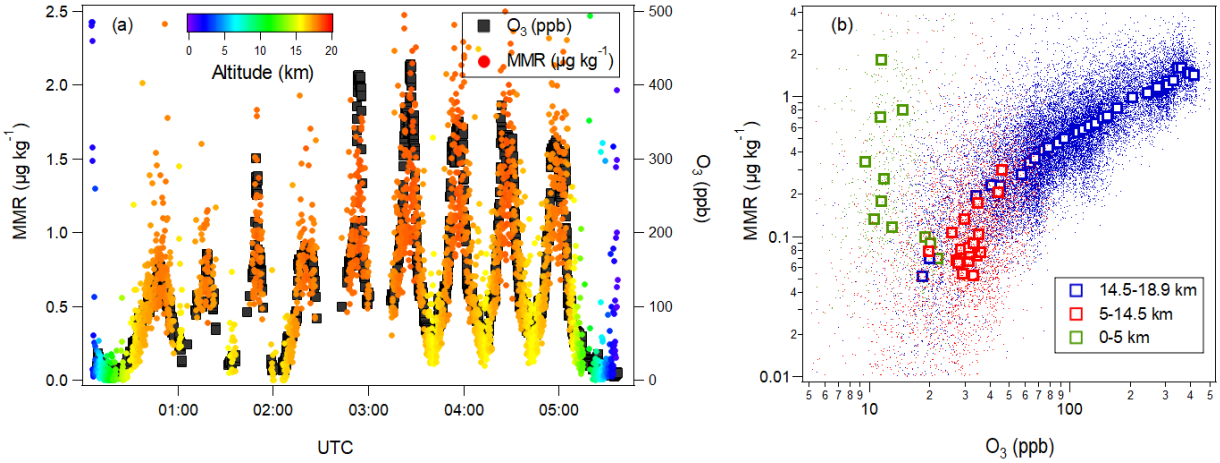

Figure 3. **(a)** Example time series of aerosol MMR and O_3 for the October 18 measurements. The gaps indicate ice-influenced data that were excluded from the analysis. **(b)** Scatter plot of MMR vs O_3 for the 0–5 km (layer I), 5–14.5 km (layer II), and 14.5–18.9 km (layer III) measurements. Individual data points are shown by the dots and the averages are shown by the solid squares Logarithmic scales are used to make the small values visible.

We used a one-dimensional column model (over the flight region) and tracer analysis to examine these processes. The model calculates the vertical distribution of O_3 within the TTL, considering a constant slow vertical ascent rate of 0.25 mm s^{-1} (Park et al., 2010; Avallone and Prather 1996) of air in the TTL and assuming it evolves in isolation (Supporting Information). Remarkably, the calculated vertical profile of O_3 closely aligns with the observed O_3 profile (Fig. 4a). This result is in line with earlier investigations that yielded similar results using a column model (Avallone and Prather 1996) and with research that assumed the tropics are isolated from extra-tropics when explaining the annual cycles of ozone above the tropical tropopause (Randel et al., 2007; Schoeberl et al., 2008). However, we acknowledge the simplicity of the model. For example, the model does not consider the chemistry of nitrogen oxides (NO and NO_2; not measured during POSIDON) and O_3, which could be important in the TTL O_3 abundance (Nussbaumer et al., 2023), and uncertainties exist in the assumed ascent rate. On the other hand, the tracer analysis shows evidence of stratospheric in-mixing. Fig. S4 shows that N_2O was anticorrelated with O_3 in the TTL during POSIDON. The observed negative correlation indicates that the sampled TTL air included a contribution from mixing of stratospheric origin (Folkins et al., 1999). This is because the strong UV radiation at higher altitudes in the stratosphere photolyzes N_2O while leading to O_3 production, resulting in an anticorrelation of N_2O and O_3 (Assonov et al., 2013). In contrast, N_2O in the troposphere is inert and uniformly distributed, thus correlation of N_2O with O_3 is not expected and not observed below the TTL during our measurements. The synthesis of modeling and tracer analysis indicates contributions from both chemical production and stratospheric in-mixing to TTL

O_3. Given the strong correlation between O_3 and aerosols in the TTL, these results suggest that TTL aerosols may also come from a combination of these chemical and physical processes.

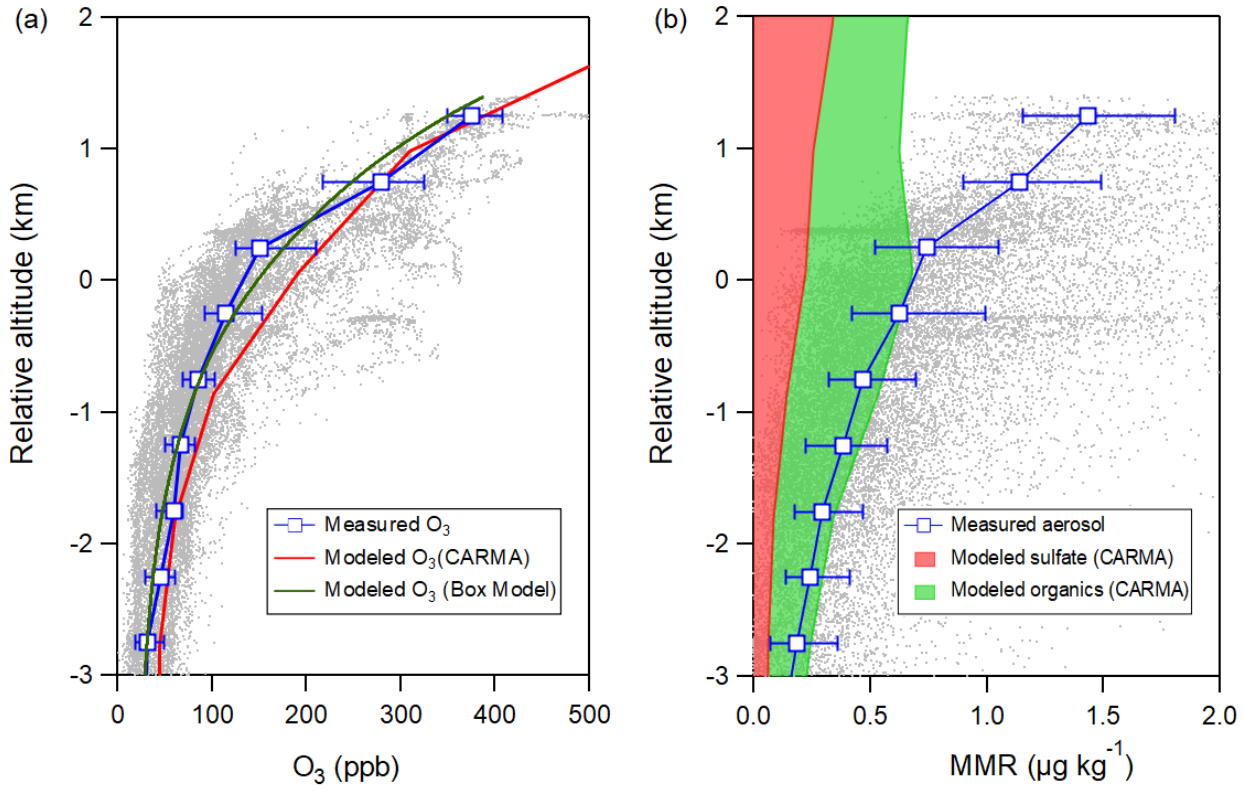

Figure 4. Comparison of modeling results to measurements for **(a)** O_3 and **(b)** aerosol MMR. Individual measurement points are shown by the grey dots. The median values and the 25th and 75th percentiles are shown by the blue line-square symbols and the error bars. The y-axis represents altitude relative to the tropopause.

To investigate the chemical composition of TTL aerosol, we employed the CARMA model embedded in CESM to simulate the aerosol formation and growth processes. The model reproduced the O_3 profile reasonably well (Fig. 4a). Our model results suggest that sulfate aerosol exhibits a consistent increase with altitude, whereas organic aerosol displays an ascending trend below the tropopause but declines above it. Moreover, our modeled vertical profile of the total aerosol MMR demonstrates good agreement with the in situ measurements (Fig. 4b) below the tropopause, with organic aerosol constituting the significant fraction of the aerosol mass. These modeling results imply that sulfur alone is insufficient to explain the observed aerosol mass, and organic precursors may play a pivotal role in the formation and/or growth of TTL aerosols under low-temperature conditions. This finding aligns with previous findings from TTL measurements during the Pre-AVE and CR-AVE campaigns over Southwest Central America in boreal winter (Froyd et al., 2009), which highlighted the prevalence of organic-sulfate particles as the most abundant particle type in the TTL and lower stratosphere. We note that the model underestimates the aerosol mass above the tropopause, with the difference increasing with altitude within the TTL,

reaching 60% at an altitude of 1 km above the CPT. Additional research is needed to understand this discrepancy.

We postulate that TTL aerosols are likely generated through the processes of new particle formation and subsequent growth following convective outflow in the upper troposphere (Williamson et al., 2019). The observed aerosol number size distribution in the TTL suggests particle growth with increasing altitude (Fig. S5), although obtaining measurements of smaller particles would enhance our understanding. During convective transport, soluble species are effectively removed, whereas the insoluble and weakly soluble species can endure washout and gradually ascend upward, with minimal loss, to reach the stratosphere (Bechara et al., 2010). The TTL, characterized by low temperature, low particle surface area density, and high relative humidity, provides ideal conditions for new particle formation and growth. Multiple studies have proposed the upper troposphere as the primary nucleation region (Brock et al., 1995; Weigel et al., 2011), and investigations have revealed the involvement of organics in new particle formation and initial growth in the remote tropical upper troposphere (Kupc et al., 2020). Future measurements analyzing the composition of oxidized organic species will enhance our understanding of particle formation and growth pathways. Exceptional overshooting that crosses the tropical tropopause could also affect the aerosol abundance in the TTL (Vernier et al., 2011). This possibility is examined using H_2O as a tracer. The θ-H_2O profile displayed no spikes above the tropopause (Fig. S6), suggesting the absence of overshooting during the measurements.

The prevalence of secondary aerosol formation as the primary factor influencing TTL aerosol abundance is in line with the strong correlation between TTL aerosol mass and O_3 in our measurements. Building upon this observation and the underlying mechanisms, we further derived an empirical parameterization of aerosol MMR as a function of O_3 in the TTL using linear regression. The derived relationship is expressed as MMR ($\mu g\ kg^{-1}$) = $0.0074(\pm 2.2 \times 10^{-4}) \times O_3$ (ppb) + 0.23 ($\pm$0.049), accounting for the 50% mass that was not measured by the POPS instrument. This parameterization could be used to estimate TTL aerosol abundance and for validation of modeled results.

4 Conclusions

Our aircraft measurements conducted over the western Pacific revealed a vertically stratified aerosol distribution comprised of three distinct layers. The lower-troposphere layer, ranging from 0 to 5 km in altitude, exhibited a decrease in aerosol mass with height, primarily influenced by surface-level emissions. The layer between 5 and 14.5 km displayed consistently low aerosol concentrations with minimal variability, indicating effective aerosol removal through deep convection processes. In the TTL, we observed an enhanced aerosol mass that exhibited a strong correlation with O_3. The modeling and tracer analysis suggest that TTL O_3 and aerosols likely originate from a combination of chemical production and stratospheric in-mixing processes. Furthermore, based on the linear relationship observed between aerosol MMR and O_3 in the TTL, we derived an empirical parameterization that allows for the estimation of aerosol MMR as a

function of O_3. This parameterization holds potential for validating the simulated TTL aerosol abundance in global models, enabling the simulation of the climate impacts of TTL aerosols.

Our study also highlights the challenge of accurately predicting aerosol mass, particularly above the tropopause, even for the most advanced models. This underscores the existence of significant gaps in our understanding of the origin and formation mechanisms of aerosols in the TTL. To achieve a more comprehensive understanding of TTL aerosol, it is crucial to conduct future measurements that encompass detailed aerosol chemical composition and gas-phase precursors across different locations and seasons. These endeavors will help diagnose potential deficiencies in the models and validate the modeling results. Consequently, they will lead to an improved comprehension of TTL aerosols and facilitate a predictive understanding of their effects on stratospheric chemistry, clouds, and climate.

Acknowledgement

We appreciate the funding support from ERB. We would like to thank Paul Lawson from APEC Incorporated for the help with collecting the FCDP data. We are also thankful to Paul Bui for providing the MMS data.

Data Availability Statement

The aircraft measurements during the POSIDON field campaign are available through the NASA ESPO Data Archive: https://espoarchive.nasa.gov/archive/browse/posidon/WB57

References

Abalos, M., Randel, W.J., Kinnison, D.E., & Serrano, E. (2013). Quantifying tracer transport in the tropical lower stratosphere using WACCM. *Atmos. Chem. Phys*., 13, 10591–10607.

Abalos et al., Ploeger, F., Konopka, P., Randel, W. J., & Serrano, E. (2013). Ozone seasonality above the tropical tropopause: reconciling the Eulerian and Lagrangian perspectives of transport processes, *Atmos. Chem. Phys.*, 13, 10787–10794.

Andreae, M. O., Afchine, A., Albrecht, R., Holanda, B. A., Artaxo, P., Barbosa, H. M. J., et al. (2018). Aerosol characteristics and particle production in the upper troposphere over the Amazon Basin. *Atmo. Meas. Tech.*, 18, 921–961.

Assonov, S. S., Brenninkmeijer, C. A. M., Schuck, T. & Umezawa, T. (2013). N_2O as a tracer of mixing stratospheric and tropospheric air based on CARIBIC data with applications for CO_2. *Atmos. Environ.*, 79, 769–779.

Avallone, L. M., & Prather, M., J. (1996). Photochemical evolution of ozone in the lower tropical stratosphere. *J. Geophys. Res.*, 101. https://doi.org/10.1029/95JD03010.

Bechara, J., Borbon, A., Jambert, C., Colomb, A., & Perros, P. E. (2010). Evidence of the impact of deep convection on reactive volatile organic compounds in the upper tropical troposphere during the AMMA experiment in West Africa. *Atmos. Chem. Phys.*, 10, 10321–10334.

Brock, C. A., Hamill, P., Wilson, J. C., Jonsson, H. H., & Chan, K. R. (1995). Particle formation in the upper tropical troposphere : A Source of Nuclei for the Stratospheric Aerosol. *Science*, 270, 1650–1653.

Chan, K. R., Scott, S. G., & Bui, T. P. (1989). Temperature and horizontal wind measurements on the ER-2 aircraft during the 1987 airborne Antarctic ozone experiment. *J. Geophys. Res.*, 94, 11573–11587. https://doi.org/10.1029/JD094iD09p11573.

Cui, Y. Y., Liu, S., Bai, Z., Bian, J., Li, D., Fan, K. et al. (2018). Religious burning as a potential major source of atmospheric fine aerosols in summertime Lhasa on the Tibetan Plateau. *Atmos. Environ.*, 181, 186–191.

Crutzen, P. J., Lawrence, M. G., & Poschl, U. (1999). On the background photochemistry of tropospheric ozone. *Tellus*, 51A-B, 123–146.

Folkins, I. & Martin, R. V. (2005). The vertical structure of tropical convection and its impact on the budgets of water vapor and ozone. *J. Atmos. Sci.*, 62(5), 1560–1573.

Folkins, I., Loewenstein, M., Podolske, J., & Oltmans, J. (1999). A barrier to vertical mixing at 14 km in the tropics: Evidence from ozonesondes and aircraft measurements. *J. Geophys. Res.*, 104, 22095–22102. https://doi.org/10.1029/1999JD900404.

Folkins, I., Braun, C., Thompson, A. M., & Witte, J. (2002). Tropical ozone as an indicator of deep convection. *J. Geophys. Res. Atmos.*, 107(13), 1–10. https://doi.org/10.1029/2001JD001178.

Froyd, K. D., Murphy, D. M., Sanford, T. J., Thomson, D. S., Wilson, J. C., Pfister, L., & Lait, L. (2009). Aerosol composition of the tropical upper troposphere. *Atmos. Chem. Phys.*, 9, 4363–4385.

Fueglistaler, S., M. Bonazzola, P. H. Haynes, & Peter T. (2005). Stratospheric water vapor predicted from the Lagrangian temperature history of air entering the stratosphere in the tropics. *J. Geophys. Res.*, 110, D08107, doi:10.1029/2004JD005516.

Fueglistaler, S., Dessler, A. E., Dunkerton, T. J., Folkins, I., Fu, Q., & Mote, P. W. (2009). Tropical tropopause layer. *Rev. Geophys.*, 47, https://doi.org/10.1029/2008RG000267.

Gao, R. S., Ballard, J., Watts, L. A., Thornberry, T. D., Ciciora, S. J., McLaughlin, R. J., & Fahey, D. W. (2012). A compact, fast UV photometer for measurement of ozone from research aircraft, *Atmos. Meas. Tech.*, 5(9), 2201–2210. https://doi.org/10.5194/amt-5-2201-2012.

Gao, R. S., Telg, H., McLaughlin, R. J., Ciciora, S. J., Watts, L. A., Richardson, M. S. et al. (2016). A light-weight, high-sensitivity particle spectrometer for $PM_{2.5}$ aerosol measurements. *Aerosol Sci. Technol.*, 50, 88–99..

Gettelman, A. & Forster, P. M. d. F. (2002). A climatology of the tropical tropopause layer. *J. Meteorol. Soc. Japan*, 80(4B), 911–924. https://doi.org/10.2151/jmsj.80.911.

Hong, Y., Liu, G., & Li, J.-L. F. (2016). Assessing the radiative effects of global ice clouds based on CloudSat and CALIPSO measurements. *J. Climate*, 7651–7674, https://doi.org/10.1175/JCLI-D-15-0799.1.

Jensen, E. J., Diskin, G., Lawson, R. P., Lance, S., Bui, T. P., Hlavka, D. et al. (2013). Ice nucleation and dehydration in the tropical tropopause layer. *Proc. Natl. Acad. Sci.*, 110(6). https://doi/org/10.1073/pnas.1217104110.

Jonsson, H. H., Wilson, J. C., Brock, C. A., Knollenberg, R. G., Newton, R., Dye, J. E. et al. (1995). Performance of a focused cavity aerosol spectrometer for measurements in the stratosphere of particle size in the 0.06-2.0-µm-dimaeter range. *J. Atmos. Ocean. Technol.*, 12, 115–129.

Konopka, P., Grooß, J.-U., Ploeger, F., & Müller, R. (2009). Annual cycleof horizontal in-mixing into the lower tropical stratosphere. *J. Geophys. Res.*, 114, D19111. https://doi.org/10.1029/2009JD011955.

Konopka, P., Grooß, J.-U., Günther, G., Ploeger, F., Pommrich, R., Müller, R., & Livesey, N. (2010). Annual cycle of ozone at and above thetropical tropopause: Observations versus simulations with the ChemicalLagrangian Model of the Stratosphere (CLaMS). *Atmos. Chem. Phys.*,10, 121–132.

Krejci, R., Stro, J., Reus, M. De, Hoor, P., Williams, J. & Fischer, H. (2003). Evolution of aerosol properties over the rain forest in Surinam , South America , observed from aircraft during the LBA-CLAIRE 98 experiment. *J. Geophys. Res.-Atmos*, 108, 1–17. doi:10.1029/2001JD001375.

Kupc, A., Williamson, C. J., Hodshire, A. L., Kazil, J., Ray, E., Bui, T. P. et al. (2020). The potential role of organics in new particle formation and initial growth in the remote tropical upper troposphere. *Atmos. Chem. Phys.*, 20, 15037–15060.

Lance, S., Brock, C. A., Rogers, D., Gordon, J. A., & Oceanic, N. (2010). Water droplet calibration of the Cloud Droplet Probe (CDP) and in-flight performance in liquid , ice and mixed-phase clouds during ARCPAC. *Atmo. Meas. Tech.*, 3, 1683–1706. https://doi:10.5194/amt-3-1683-2010.

Mcfarquhar, G. M., Um, J., Freer, M., Baumgardner, D., Kok, G. L., & Mace, G. (2007). Importance of small ice crystals to cirrus properties: Observations from the Tropical Warm Pool International Cloud Experiment. *Geophys. Res. Lett.*, 34, 1–6. https://doi.org/10.1029/2007GL029865.

Liu, S., Liu, C. C., Froyd K. D., Schill, G. P., Murphy, D. M., Bui, T. P. et al. (2021). Sea spray aerosol concentration modulated by sea surface temperature. *Proc. Natl. Acad. Sci.*, 118(9), https://doi.org/10.1073/pnas. 2020583118.

Mclinden, C. A., McConnell, J. C., McElroy, C. T., & Griffioen, E. (1999). Observations of stratospheric aerosol using CPFM polarized limb radiances. *J. Atmos. Sci.*, 56, 233–240.

Murphy, D. M., Cziczo, D. J., Hudson, P. K., Thomson, D. S., Wilson, J. C., Buseck, P. R. et al. (2004). Particle generation and resuspension in aircraft inlets when flying in clouds particle

generation and resuspension in aircraft inlets when flying in clouds. *Aerosol Sci. Technol.*, 38, 401–409. https://doi.org/10.1080/02786820490443094.

Nussbaumer, C. M., Fischer, H., Lelieveld, J., & Pozzer, A. (2003). What controls ozone sensitivity in the upper tropical troposphere? *Atmos. Chem. Phys*., 23, 12651–12669.

Penner, J. E., Chen, Y., Wang, M., & Liu, X. (2009). Possible influence of anthropogenic aerosols on cirrus clouds and anthropogenic forcing. *Atmos. Chem. Phys*., 9(3), 879–896. https://doi.org/10.5194/acp-9-879-2009.

Ploeger, F., fueglistaler, S., Grooß, J.-U., Günther, G., Konopka, P., Liu, Y. S., et al. (2011). Insight from ozone and water vapour on transportin the tropical tropopause layer (TTL). *Atmos. Chem. Phys*, 11, 407–419.

Ploeger, F., Konopka, P., Müller, R., Fueglistaler, S., Schmidt, T., Manners, J. C. et al. (2012). Horizontal transport affecting trace gas seasonality in the Tropical Tropopause Layer (TTL). *J. Geophys. Res.*, 117, D09303. https://doi.org/10.1029/2011JD017267.

Prather, M. J. (2009). Tropospheric O_3 from photolysis of O_2. *Geophys. Res. Lett.*, 36. https://doi:10.1029/2008GL036851.

Randel, W. J. & Jensen, E. J. (2013). Physical processes in the tropical tropopause layer and their roles in a changing climate. *Nat. Geosci.*, 6, 169–176. https://doi/org10.1038/ngeo1733.

Randel, W. J., Park, M., & Wu, F. (2007). A large annual cycle in ozone above the tropical tropopause linked to the Brewer-Dobson circulation. *J. Atmos. Sci.*, 4479–4488.

de Reus, M., Krejci, R., Williams, J., Fischer, H., Scheele, R. & Strom, J. (2001). Vertical and horizontal distributions of the aerosol number concentration and size distribution over the northern Indian Ocean. *J. Geophys. Res.-Atmos*, 106, 629–641. https://doi.org/10.1029/2001JD900017.

Gelaro, R., McCarty, W., Suarez, M. J., Todling, R., Molod, A., Takacs, L. et al. (2017). The Modern-Era Retrospective Analysis for Research and Applications, Version 2 (MERRA-2). *J. Climate*, 5419–5454.

Rollins, A. W., Thornberry, T. D., Watts, L. A., Yu, P., Rosenlof, K. H., Mills, M. et al. (2017). The role of sulfur dioxide in stratospheric aerosol formation evaluated by using in situ measurements in the tropical lower stratosphere. *Geophys. Res. Lett*., 4280–4286. https:// doi.org/10.1002/2017GL072754.

Sargent, M. R., Smith, J. B., Sayres, D. S., & Anderson, J. G. (2014). The roles of deep convection and extratropical mixing in the tropical tropopause layer: An in situ measurement perspective. *J. Geophys. Res.-Atmos*, 12355–12371. https://doi.org/10.1002/2014JD022157.

Schoeberl, M. R., Douglass, A. R., Newman, P. A., Lait, L. R., Lary, D., Waters, J. (2008). QBO and annual cycle variations in tropical lower stratosphere trace gases from HALOE and Aura MLS observations. *J. Geophys. Res.*, 113, D05301. https://doi.org/10.1029/2007JD008678.

Schwarz, J. P., Gao, R. S., Fahey, D. W., Thomson, D. S., Watts, L. A., Wilson, J. C. (2006). Single-particle measurements of midlatitude black carbon and light-scattering aerosols from the boundary layer to the lower stratosphere. *J. Geophys. Res*., 111. https://doi.org/10.1029/2006JD007076, doi:10.1029/2006JD007076.

Scott, S. G., Bui, P. T. & Chan, R. K. (1990). The meteorological measurement system on the NASA ER-2 aircraft. *J. Atmos. Ocean. Technol.*, 7, 525–540.

Stratosphere-troposphere Processes and their Role in Climate (SPARC), Assessment of Stratospheric Aerosol Properties (ASAP), WCRP-124, WMO/TD No. 1295, SPARC Rep. 4, 2006.

Sunilkumar, S. V., Muhsin, M., Venkat Ratnam, M., Parameswaran, K., Krishna Murthy, B. V., & Emmanuel, M. (2017). Boundaries of tropical tropopause layer (TTL): A new perspective based on thermal and stability profiles. *J. Geophys. Res*., 741–754, 2017. https://doi.org/10.1002/2016JD025217.

Thornberry, T. D., Rollins, A. W., Gao, R. S., Watts, L. A., Ciciora, S. J., McLaughlin, & Fahey, D. W. (2015). A two-channel, tunable diode laser-based hygrometer for measurement of water vapor and cirrus cloud ice water content in the upper troposphere and lower stratosphere. *Atmos. Meas. Tech.*, 8, 211-224. https://doi.org/10.5194/amt-8-211-2015.

Tolbert, A., Rossi, J. M. & Golden, D. M. (1988). Heterogeneous interactions of chlorine nitrate, hydrogen chloride, and nitric acid with sulfuric acid surfaces at stratospheric temperatures. *Geophys. Res. Lett.*, 15, 847–850. https://doi.org/10.1029/GL015i008p00847.

Toon, O. B., Turco, R. P., Westphal, D., Malone, R., & Liu, M. (1988). A multidimensional model for aerosols—Description of computational analogs. *Journal of the Atmospheric Sciences*, 45(15), 2123–2144.

Vernier, J., Pommereau, J., Thomason, L. W., Pelon, J., Garnier, A., Deshler, T. et al. (2011). Overshooting of clean tropospheric air in the tropical lower stratosphere as seen by the CALIPSO lidar. *Atmos. Chem. Phys.*, 9683–9696. https://doi.org/10.5194/acp-11-9683-2011.

Weigel, R., Borrmann, S., Kazil, J., Minikin, A., Stohl, A., Wilson, J. C. et al. (2011). In situ observations of new particle formation in the tropical upper troposphere: The role of clouds and the nucleation mechanism. *Atmos. Chem. Phys.*, 11, 9983–10010. https://doi.org/10.5194/acp-11-9983-2011.

Weigel, R., Mahnke, C., Baumgartner, M., Dragoneas, A., Vogel, B., Ploeger, F. et al. (2021). In situ observation of new particle formation (NPF) in the tropical tropopause layer of the 2017 Asian monsoon anticyclone – Part 1:Summary of StratoClim results. *Atmos. Chem. Phys*., 21, 11689–11722.

Williamson, C. J., Kupc, A., Axisa, D., Bilsback, K. R., Bui, T., Campuzano-jost, P. (2019). A large source of cloud condensation nuclei from new particle formation in the tropics. *Nature*, 574,

399–403. https://doi.org/10.1038/s41586-019-1638-9.

Yan, X., Ho, C., Zheng, Q., & Klemas, V. (1992). Temperature and size variabilities of the western pacific warm pool. *Science,* 258, 1643–1645.

Yu, P., Toon, O. B., Bardeen, C. G., Mills, M. J., Fan, T., English, J. M., & Neely, R. R. (2015). Evaluations of tropospheric aerosol properties simulated by the community Earth system model with a sectional aerosol microphysics scheme. *Journal of Advances in Modeling Earth Systems, 7*(2), 865–914.

Yu, P., Rosenlof, K. H., Liu, S., Telg, H., Thornberry, T. D., Rollins, A. W. et al. (2017). Efficient transport of tropospheric aerosol into the stratosphere via the Asian summer monsoon anticyclone. *Proc. Natl. Acad. Sci.*, 114(27), 6972–6977. https://doi.org/10.1073/pnas.1701170114.

Yu, P., Froyd, K. D., Portmann, R. W., Toon, O. B., Freitas, S. R., Bardeen, C. G. et al. (2019). Efficient in-cloud removal of aerosols by deep convection. Geophysical Research Letters, 46. https://doi.org/10.1029/2018GL080544.

Zhao, J., & Turco, R. P. (1995). Nucleation simulations in the wake of a jet aircraft in stratospheric flight. *J. Aerosol Sci.*, 26, 779–795.

Supporting Information for

Enhanced Aerosol Mass in the Tropical Tropopause Layer Linked to Ozone Abundance

Shang Liu[1,*], Troy D. Thornberry[2], Pengfei Yu[3], Sarah Woods[4], Karen H. Rosenlof[2], and Ru-Shan Gao[2,*]

[1]Department of Civil and Environmental Engineering, Northeastern University, Boston, MA 02115, USA
[2]NOAA Chemical Sciences Laboratory, Boulder, CO, USA
[3]Institute for Environmental and Climate Research, Jinan University, Guangzhou, China
[4]Earth Observing Laboratory, National Center for Atmospheric Research (NCAR), Boulder, CO

*Correspondence author: shang.liu@northeastern.edu, rushan.gao@noaa.gov

1. Model calculation of ozone profile in the TTL

The natural ozone chemical cycle is described by the Chapman reactions as follows:

$$O_2 \xrightarrow{h\nu} O + O \quad \text{(R1)}$$

$$O + O_2 \xrightarrow{M} O_3 \quad \text{(R2)}$$

$$O_3 \xrightarrow{h\nu} O + O_2 \quad \text{(R3)}$$

$$O + O_3 \rightarrow O_2 + O_2 \quad \text{(R4)}$$

The rate equations for [O] and [O_3] are

$$\frac{d[O]}{dt} = 2j_{O_2} - k_2[O][O_2][M] + j_{O_3}[O_3] - k_4[O][O_3] \quad (1)$$

$$\frac{d[O_3]}{dt} = k_2[O][O_2][M] - j_{O_3}[O_3] - k_4[O][O_3] \quad (2)$$

Combining (1) and (2) we obtain

$$\frac{d[O + O_3]}{dt} = 2j_{O_2}[O_2] - 2k_4[O][O_3] \quad (3)$$

Since [O] $\ll$ [O_3], equation (3) can be written as

$$\frac{d[O_3]}{dt} = 2j_{O_2}[O_2] - 2k_4[O][O_3] \quad (4)$$

The fast interconversion between O and O_3 (R2 and R3) leads to the following relationship between O and O_3 concentrations (Seinfeld and Pandis 2016):

$$\frac{[O]}{[O_3]} = \frac{j_{O_3}}{k_2[O_2][M]} \quad (5)$$

Therefore the production rate of O_3 is expressed as

$$\frac{d[O_3]}{dt} = 2j_{O_2}[O_2] - \frac{2k_4 j_{O_3}[O_3]^2}{k_2[O_2][M]} \quad (6)$$

Where

- $k_2 = 6.0 \times 10^{-34}(T/300)^{-2.4}$, with an average of 1.7 x 10^{-33} cm^6 $molec^{-2}$ s^{-1} in the TTL.
- $k_4 = 8.0 \times 10^{-12}\, exp(-2060/T)$, with an average of 2.0 x 10^{-16} cm^3 $molec^{-1}$ s^{-1} in the TTL.
- j_{O_3} ranges from 3 x 10^{-4} s^{-1} (SZA=85°) to 6.5 x 10^{-4} s^{-1} at SZA = 0° in the TTL (Seinfeld and Pandis, 2016, Fig. 4.13 on p. 112).
- j_{O_2} ranges with increasing altitude from 2.0 x 10^{-15} s^{-1} to 7 x 10^{-14} s^{-1} at SZA = 0° in the TTL (2016, Fig. 4.12 on p.111).

From the observations we have the following average concentrations:

[M] = 1.5 x 10^{18} molecules cm^{-3}
$[O_2]$ = 0.21 x [M] = 3.2 x 10^{17} molecules cm^{-3}
$[O_3]$ = 117 ppb = 1.9 x 10^{11} molecules cm^{-3}

Using the these values, we find that the first term of equation (6) is $2j_{O_2}[O_2]$ = 1.2 x 10^3–4.4 x 10^4 molecules $cm^{-3}s^{-1}$, and the second term of equation (6) is $\frac{2k_4 j_{O_3}[O_3]^2}{k_2[O_2][M]}$ = 5.3–11.5 molecules $cm^{-3}s^{-1}$, which can be neglected as it is about 1000 times smaller than the first term. Therefore the O_3 formation rate becomes

$$\frac{d[O_3]}{dt} = 2j_{O_2}[O_2] \quad (7)$$

We used the vertical profile from Seinfeld and Pandis (2016, Fig. 4.12 on p.111) and the vertical profile of $[O_2]$ calculated from the measurements to derive the ozone production rate. The calculated vertical profile of the ozone production rate is shown in Fig. S7. The O_3 concentration in the TTL is calculated as

$$[O_3]_i = [O_3]_{i-1} + \left(\frac{d[O_3]}{dt}\right)_i \cdot \Delta t_i = [O_3]_{i-1} + \left(2j_{O_2}[O_2]\right)_i \cdot \Delta t_i$$

Where *i* indicates the parameters at altitude *i*, and Δt_i (5 s) represents the time it takes the air to rise from altitude *i*-1 to altitude *i*, using a constant ascent rate of 0.25 mm s^{-1} (Park et al 2010; Avallone and Prather 1996; Seinfeld and Pandis 2016). The calculation is performed for the

altitude range of 14.5–18.9 km, with a prescribed [O_3] at 14.5 km of 28.8 ppb, which represents the average observed O_3 concentration at that altitude.

References

Park, S., Atlas, E. L., Jimenez, R., Daube, B. C., Gottlieb, E. W., Nan, J., Jones, D. B. A., Pfister, L., Conway, T. J., Bui, T. P., Gao, R. S. and Wofsy, S. C.: Vertical transport rates and concentrations of OH and Cl radicals in the Tropical Tropopause Layer from observations of CO 2 and halocarbons: implications for distributions of long- and short-lived chemical species, Atmos. Chem. Phys., 10, 6669–6684, doi:10.5194/acp-10-6669-2010, 2010.

Seinfeld, J. and Pandis, S.: Atmospheric chemistry and physics: from air pollution to climate change, Wiley, Hoboken, N. J., 2016.

Supporting Figures

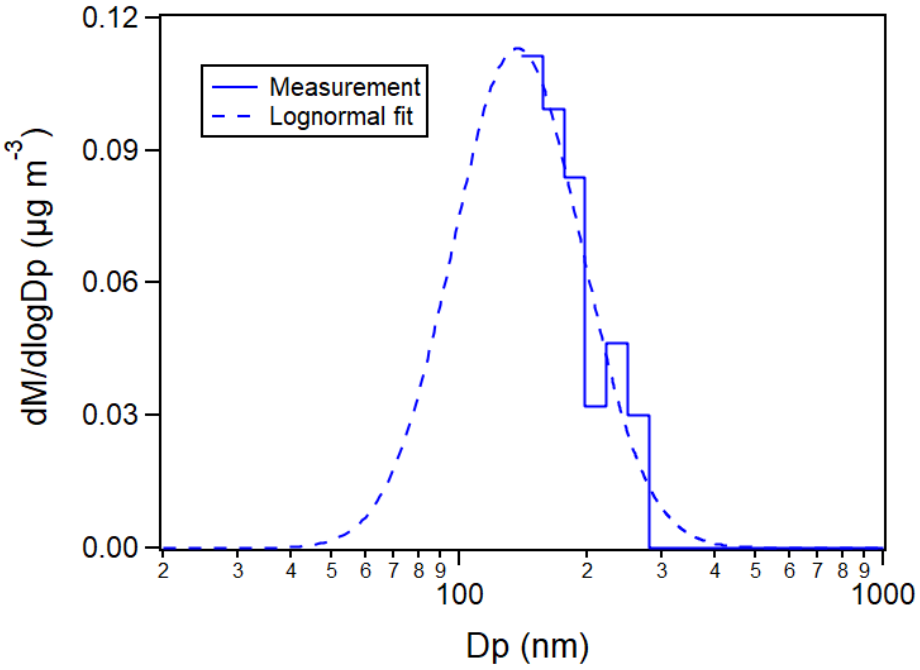

Figure S1. Lognormal fit of the average mass size distribution for the TTL measurements.

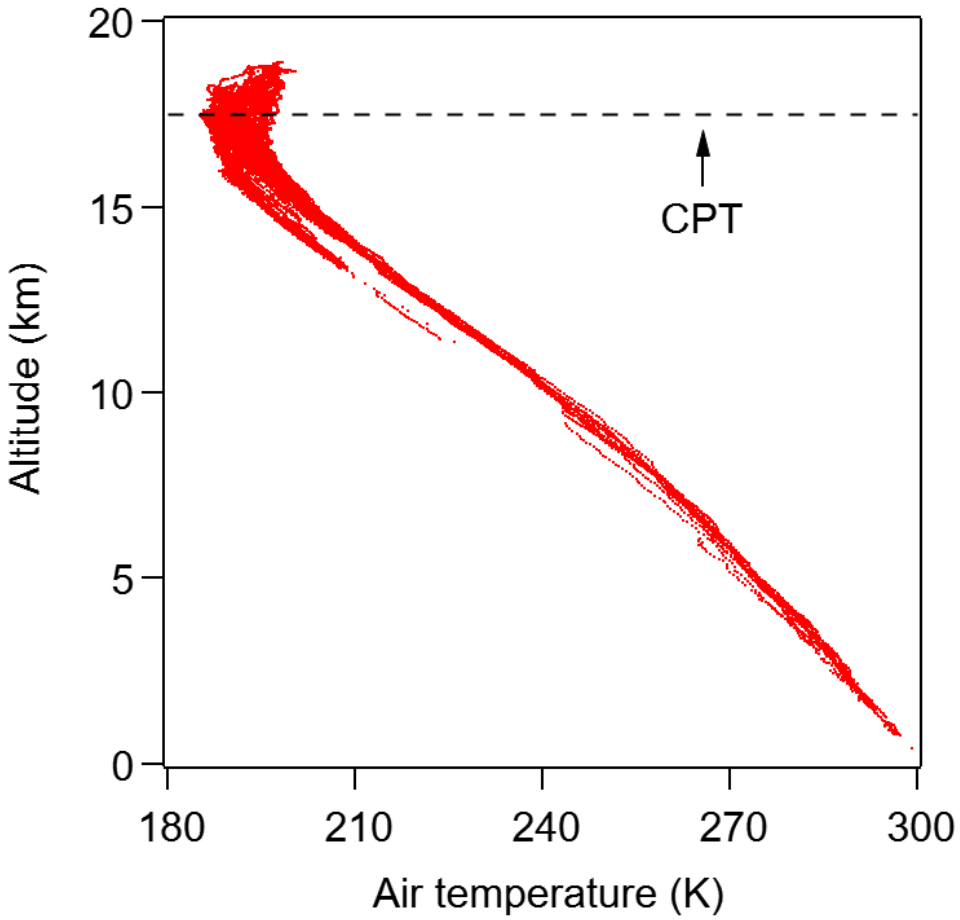

Figure S2. Vertical profile of air temperature measured from all flights.

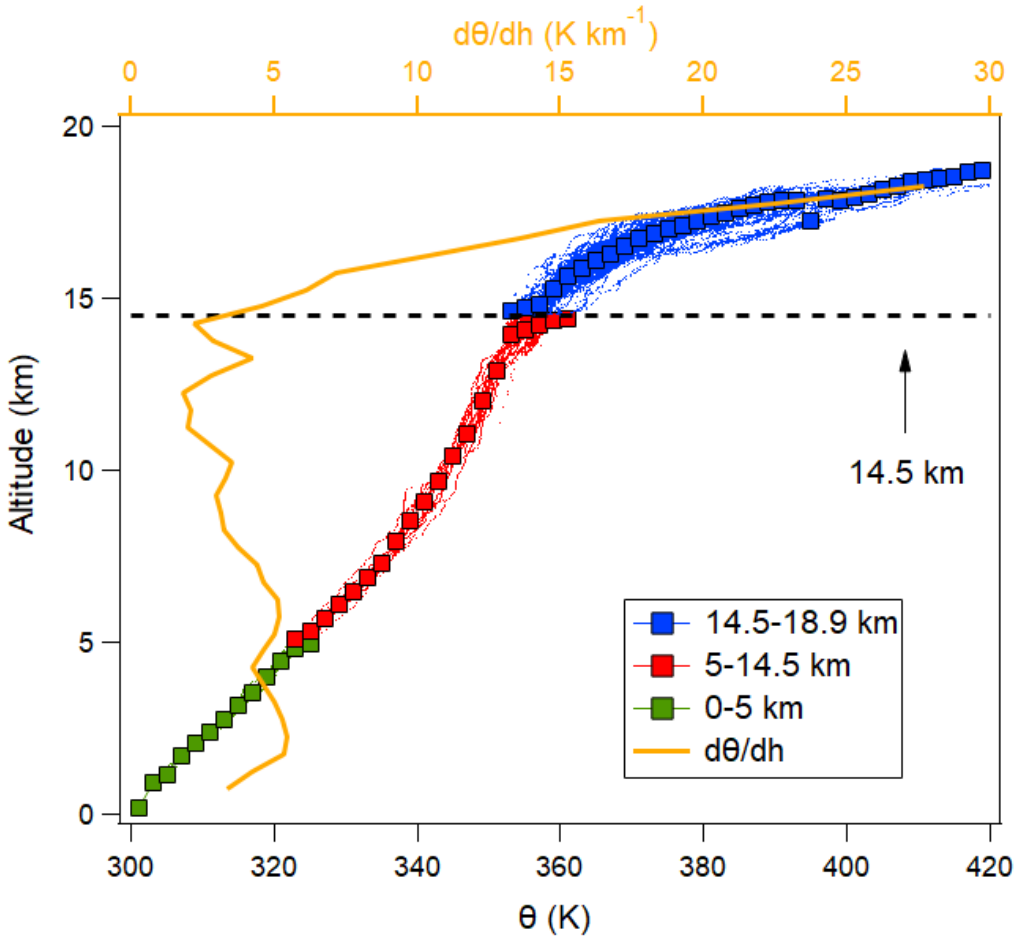

Figure S3. Vertical profiles of potential temperature (θ) and the lapse rate of θ. In the altitude-θ profile, individual data points (5-s averages) are shown by the dots and the averages (by θ of 2K) are shown by the solid squares.

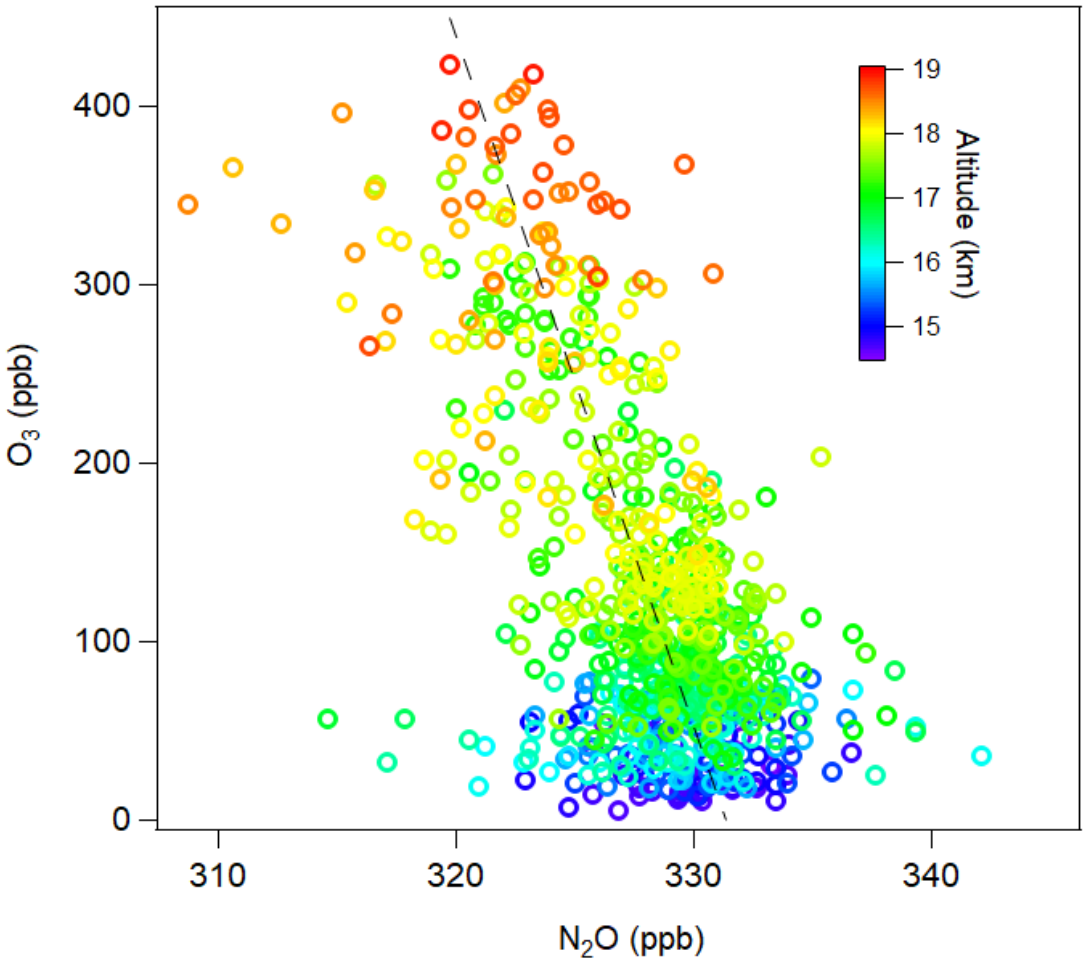

Figure S4. Scatter plot of O_3 versus N_2O in the TTL. The dashed line indicates linear fit.

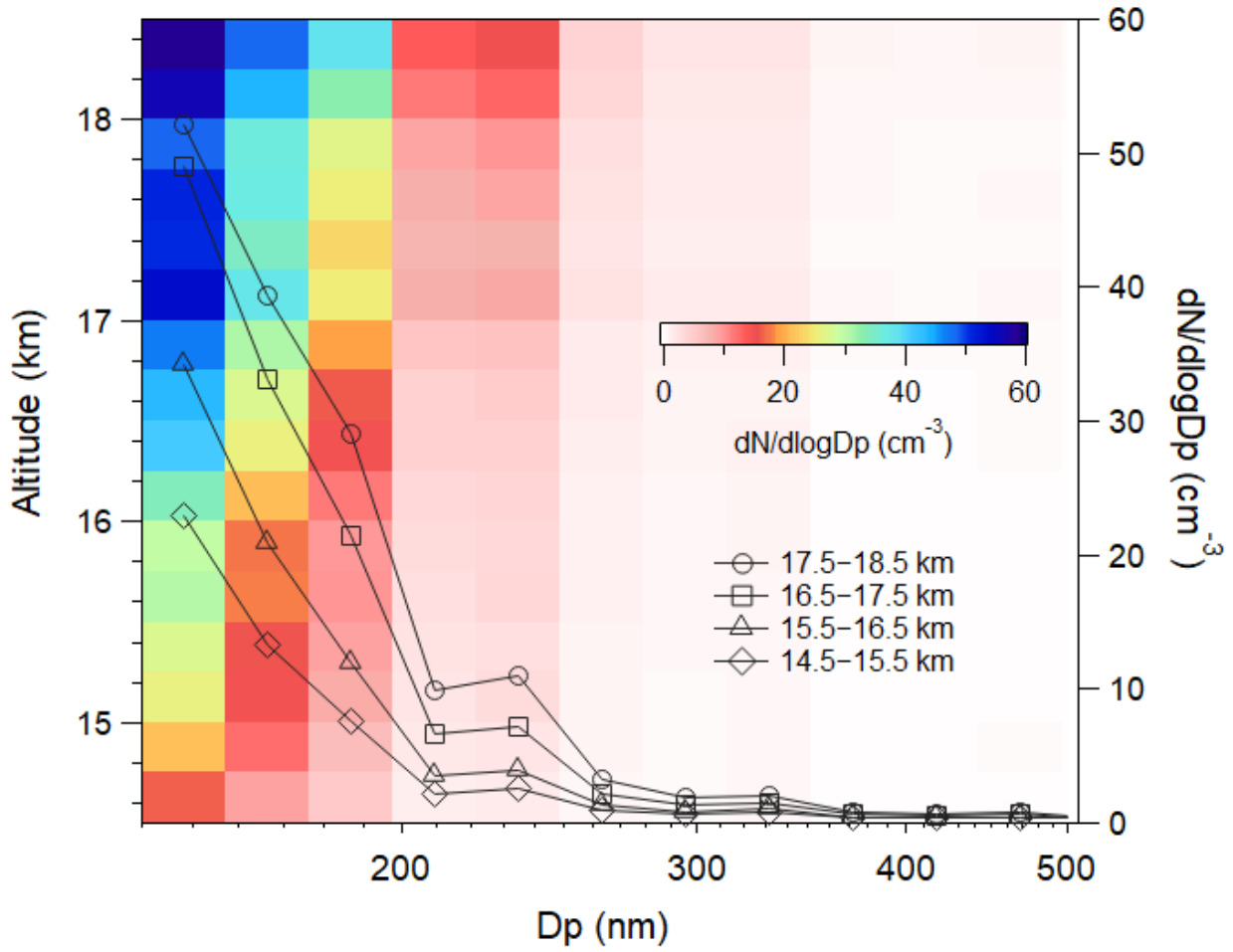

Figure S5. Image plot illustrating aerosol number size distribution with altitude in the TTL. The line and markers represent averages at various altitudinal intervals.

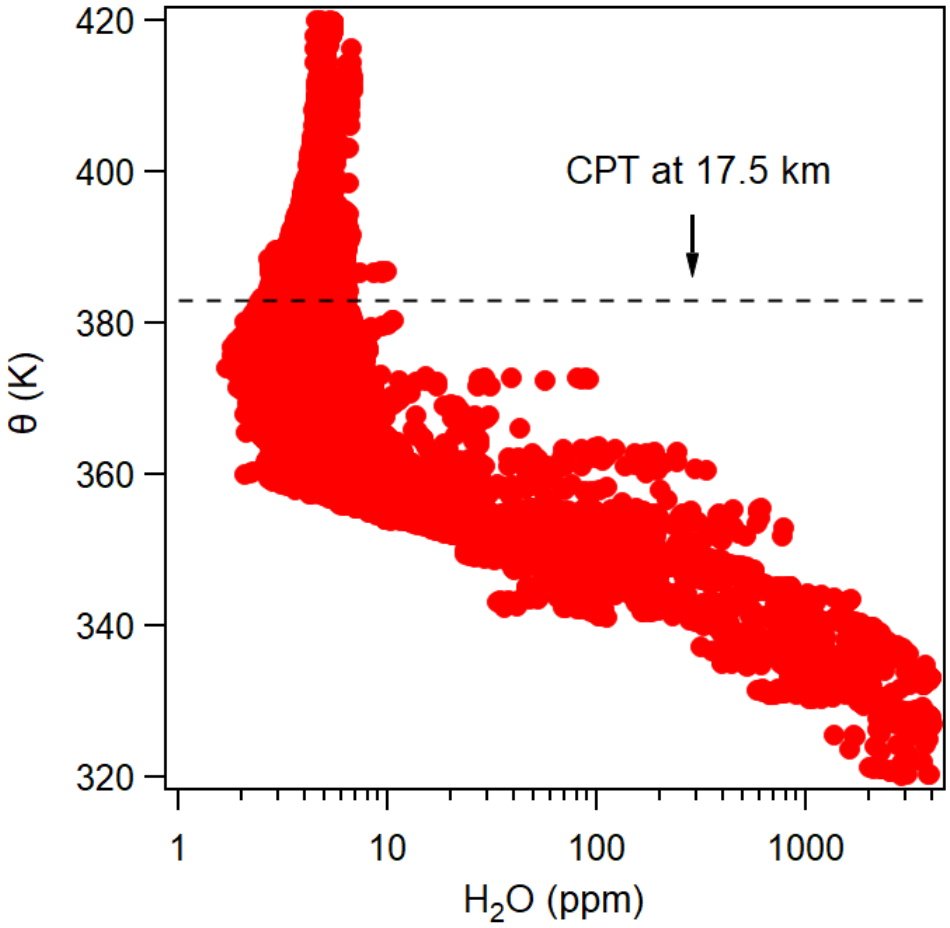

Figure S6. θ versus water vapor mixing ratio.

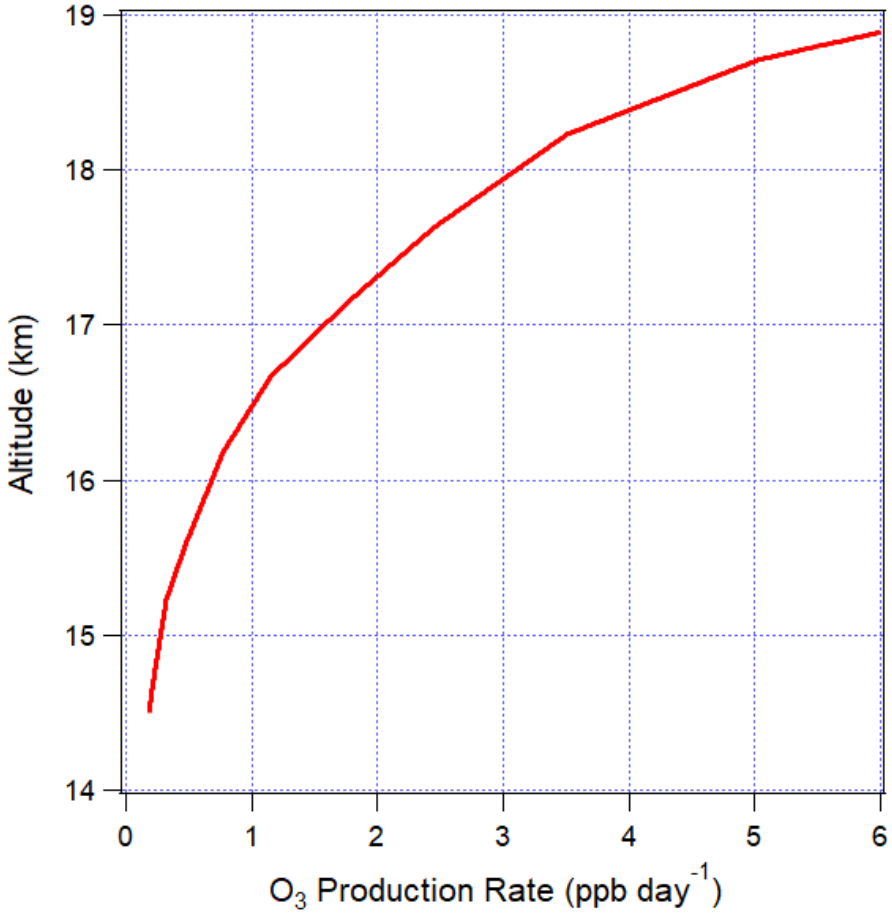

Figure S7. Calculated vertical profile of ozone production rate in the TTL.